Med

CellPress
OPEN ACCESS

Clinical and Translational Article

Immune signatures predict development of autoimmune toxicity in patients with cancer treated with immune checkpoint inhibitors

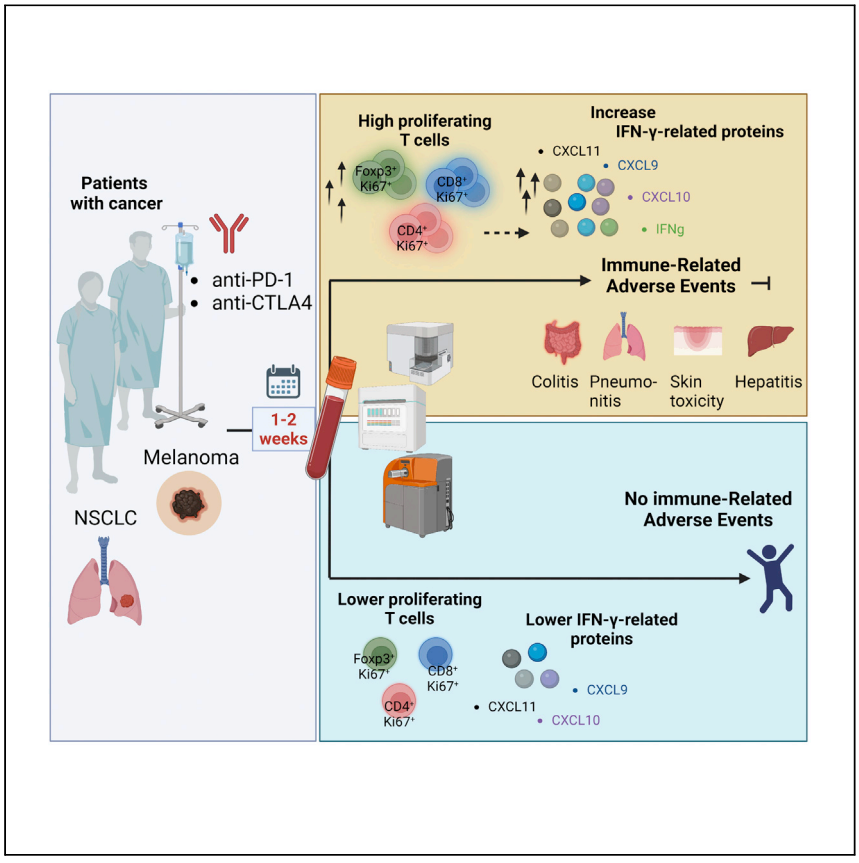

Immune checkpoint inhibitors have revolutionized cancer treatment; however, they are associated with potentially life-threatening immune-related toxicities. In a prospective multi-center study of patients with melanoma and NSCLC, Nuñez et al. identified immune signatures occurring early after the start of treatment potentially predicting the onset of adverse events.

Translation to Patients

Nicolas Gonzalo Nuñez, Fiamma Berner, Ekaterina Friebel, ..., Martin Früh, Burkhard Becher, Lukas Flatz

becher@immunology.uzh.ch (B.B.)
lukas.flatz@med.uni-tuebingen.de (L.F.)

Highlights

Systemic immune signatures shortly after the start of ICI therapy are linked to irAEs

ICI-treated patients with cancer with irAEs show an expansion of Ki-67$^+$ T cell subsets

IFN-γ and IFN-γ-related proteins CXCL9/10/11 are increased in ICI-treated patients with irAEs

Early blood ICI immune signatures may provide a predictive biomarker profile for irAEs

Nuñez et al., Med 4, 1–17
February 10, 2023 Published by Elsevier Inc.
https://doi.org/10.1016/j.medj.2022.12.007

Please cite this article in press as: Nuñez et al., Immune signatures predict development of autoimmune toxicity in patients with cancer treated with immune checkpoint inhibitors, Med (2023), https://doi.org/10.1016/j.medj.2022.12.007

Med

CellPress
OPEN ACCESS

Clinical and Translational Article

Immune signatures predict development of autoimmune toxicity in patients with cancer treated with immune checkpoint inhibitors

Nicolas Gonzalo Nuñez,[1,23] Fiamma Berner,[2,23] Ekaterina Friebel,[1,23] Susanne Unger,[1] Nina Wyss,[2,3] Julia Martinez Gomez,[4] Mette-Triin Purde,[2] Rebekka Niederer,[2,3] Maximilian Porsch,[5] Christa Lichtensteiger,[2] Rafaela Kramer,[6] Michael Erdmann,[6] Christina Schmitt,[7] Lucie Heinzerling,[6,7] Marie-Therese Abdou,[2] Julia Karbach,[8] Dirk Schadendorf,[9] Lisa Zimmer,[9] Selma Ugurel,[9] Niklas Klümper,[10,11,12] Michael Hölzel,[10,11] Laura Power,[1] Stefanie Kreutmair,[1] Mariaelena Capone,[13] Gabriele Madonna,[13] Lacin Cevhertas,[14,15] Anja Heider,[14] Teresa Amaral,[16,17] Omar Hasan Ali,[2,3,4,18] David Bomze,[2,19] Florentia Dimitriou,[4] Stefan Diem,[20] Paolo Antonio Ascierto,[13] Reinhard Dummer,[4] Elke Jäger,[8] Christoph Driessen,[20] Mitchell Paul Levesque,[4] Willem van de Veen,[14] Markus Joerger,[20] Martin Früh,[20,21] Burkhard Becher,[1,24,*] and Lukas Flatz[2,3,4,20,22,24,25,*]

SUMMARY

Background: Immune checkpoint inhibitors (ICIs) are among the most promising treatment options for melanoma and non-small cell lung cancer (NSCLC). While ICIs can induce effective anti-tumor responses, they may also drive serious immune-related adverse events (irAEs). Identifying biomarkers to predict which patients will suffer from irAEs would enable more accurate clinical risk-benefit analysis for ICI treatment and may also shed light on common or distinct mechanisms underpinning treatment success and irAEs.

Methods: In this prospective multi-center study, we combined a multi-omics approach including unbiased single-cell profiling of over 300 peripheral blood mononuclear cell (PBMC) samples and high-throughput proteomics analysis of over 500 serum samples to characterize the systemic immune compartment of patients with melanoma or NSCLC before and during treatment with ICIs.

Findings: When we combined the parameters obtained from the multi-omics profiling of patient blood and serum, we identified potential predictive biomarkers for ICI-induced irAEs. Specifically, an early increase in CXCL9/CXCL10/CXCL11 and interferon-γ (IFN-γ) 1 to 2 weeks after the start of therapy are likely indicators of heightened risk of developing irAEs. In addition, an early expansion of Ki-67$^+$ regulatory T cells (Tregs) and Ki-67$^+$ CD8$^+$ T cells is also likely to be associated with increased risk of irAEs.

Conclusions: We suggest that the combination of these cellular and proteomic biomarkers may help to predict which patients are likely to benefit most from ICI therapy and those requiring intensive monitoring for irAEs.

Funding: This work was primarily funded by the European Research Council, the Swiss National Science Foundation, the Swiss Cancer League, and the Forschungsförderung of the Kantonsspital St. Gallen.

CONTEXT AND SIGNIFICANCE

ICIs have significantly improved the treatment of a wide range of cancers. However, ICIs can cause life-threatening autoimmune side effects. There are currently no biomarkers to predict which patients are more likely to develop such side effects. Researchers at the University of Zurich, the Kantonsspital St. Gallen, and the University of Tübingen have identified early changes occurring in the blood of patients with cancer treated with ICIs. These changes predict the development of autoimmune toxicity. These findings will allow us to determine which patients are likely to benefit most from ICI therapy and those requiring intensive monitoring. Thus, the findings here may help improve care for patients with cancer by providing timely and life-saving management strategies for patients at high risk.

Please cite this article in press as: Nuñez et al., Immune signatures predict development of autoimmune toxicity in patients with cancer treated with immune checkpoint inhibitors, Med (2023), https://doi.org/10.1016/j.medj.2022.12.007

INTRODUCTION

Immune checkpoint inhibitors (ICIs) are a first-line treatment for many cancers, including melanoma and non-small cell lung cancer (NSCLC).[1–7] The potential benefits of ICI treatment for patients with cancer come at the cost of autoimmune side effects, known as ICI-induced immune-related adverse events (irAEs). The frequency of irAEs depends on the ICI used but can be as high as 70%.[8,9] irAEs can affect virtually any organ in the body[10] and typically emerge during the first few weeks of ICI therapy; however, they might occur at any point during treatment or up to several months after ICI discontinuation.[11] Severe irAEs (grades 3–4) require hospitalization, the pausing or discontinuation of therapy, and administration of immunosuppressants; in some cases, irAEs can cause death.[10,12] While there is evidence of an association between irAEs and the anti-tumor effects of ICIs,[13] the mechanisms behind their toxicity and how/whether those mechanisms can be distinguished from the anti-tumor response are poorly understood. Recent studies have investigated biomarkers for irAEs in melanoma[14,15]; however, analyses incorporating systematic approaches combining multi-omics cytometry and proteomics, as well as relevant studies in other cancer types, are lacking. Despite ongoing efforts, there currently are not any validated biomarkers available to predict which patients are more likely to develop irAEs.[16,17] In this study, we sought to identify changes in immune cell populations and cytokines over time in patients with melanoma and NSCLC treated with ICIs and to identify potential predictive biomarkers of future autoimmune toxicity.

RESULTS

The presence of ICI-induced irAEs correlated with improved patient survival

We recruited a prospective cohort comprising a group of 43 patients with melanoma and a group of 101 patients with NSCLC, all of whom were due to start treatment with ICIs. We took blood samples pre-therapy, 1 to 2 weeks after the start of therapy, and at the start of every cycle of therapy, as well as at the onset of irAEs. In addition, we collected data on the type and severity of patients' irAEs and their clinical progress during therapy (Table S1). Across the cohort, there were patients who experienced ICI-related toxicity ("Tox" subgroups), accompanied or not by tumor responsiveness to treatment (responders "Rs" and non-responders "NRs," respectively), as well as patients who did not experience toxicity ("No Tox" subgroups), but whose tumors either did or did not respond to this treatment. Specifically, within our group of patients with melanoma, we found that 63% experienced at least one irAE (Table S1), among which 19 out of 27 (70%) had ICI-responsive tumors compared with only five out of 16 patients (31%) in the No Tox subgroup, showing that irAEs were more frequent in Rs to treatment ($X^2 = 6.23$, $p = 0.01$) (Figure S1A). Although only 45% of patients with NSCLC experienced an irAE, similarly, 31 out of the 45 patients in the Tox subgroup (69%) were Rs, while in the No Tox subgroup, only 18 out of 56 patients (32%) were Rs, confirming again that irAEs were more frequent in Rs ($X^2 = 13.49$, $p = 0.0002$) (Figure S1B). Of note, the occurrence of irAEs in our cohorts is particularly high due to the strong focus on detecting and monitoring such AEs.

Among the patients with melanoma, the most frequent irAEs were autoimmune skin toxicity (21%), colitis (16%), arthritis (12%), vitiligo (12%), and hepatitis (12%) (Figure S1C). Among the patients with NSCLC, the most frequent irAEs were autoimmune skin toxicity (21%), pneumonitis (10%), arthritis (9%), colitis (8%), and thyroiditis (8%) (Figure S1D). In line with previous studies and the findings above,[9,18,19] we found that patients in both groups experiencing irAEs had

[1]Institute of Experimental Immunology, University of Zurich, Winterthurerstrasse 190, 8057 Zurich, Switzerland

[2]Institute of Immunobiology, Medical Research Center, Kantonsspital St. Gallen, St.Gallen, Switzerland

[3]Department of Dermatology, Kantonsspital St. Gallen, St. Gallen, Switzerland

[4]Department of Dermatology, University Hospital Zurich, University of Zurich, Zurich, Switzerland

[5]Department of Radiology, Kantonsspital St. Gallen, St. Gallen, Switzerland

[6]Department of Dermatology, Uniklinikum Erlangen, Deutsches Zentrum Immuntherapie (DZI), Comprehensive Cancer Center Erlangen-European Metropolitan Area of Nuremberg (CCC ER-EMN), Friedrich-Alexander-University Erlangen-Nuremberg (FAU), Erlangen, Germany

[7]Department of Dermatology, Ludwig Maximilian University of Munich, Munich, Germany

[8]Department of Oncology and Hematology, Krankenhaus Nordwest, Frankfurt, Germany

[9]Department of Dermatology, University Hospital Essen and German Cancer Consortium (DKTK), Partner Site Essen/Düsseldorf, Essen, Germany

[10]Institute for Experimental Oncology, University Hospital Bonn, Bonn, Germany

[11]Center for Integrated Oncology Cologne/Bonn, University Hospital Bonn, Bonn, Germany

[12]Department of Urology, University Hospital Bonn, Bonn, Germany

[13]Istituto Nazionale Tumori-IRCCS-Fondazione G. Pascale, Napoli, Italy

[14]Swiss Institute of Allergy and Asthma Research (SIAF), University of Zurich, Davos, Switzerland

[15]Department of Medical Immunology, Institute of Health Sciences, Bursa Uludag University, Bursa, Turkey

[16]Skin Cancer Center, Department of Dermatology, University Hospital Tübingen, Tübingen, Germany

[17]iFIT Cluster of Excellence (EXC 2180), University of Tübingen, Tübingen, Germany

[18]Department of Medical Genetics, Life Sciences Institute, University of British Columbia, Vancouver, BC, Canada

[19]Sackler Faculty of Medicine, Tel Aviv University, Tel Aviv, Israel

[20]Department of Medical Oncology and Hematology, Kantonsspital St. Gallen, St. Gallen, Switzerland

[21]Department of Medical Oncology, Inselspital, Bern University Hospital, University of Bern, Bern, Switzerland

[22]Universitäts-Hautklinik, University of Tübingen, 72016 Tübingen, Germany

[23]These authors contributed equally

[24]These authors contributed equally

[25]Lead contact

*Correspondence: becher@immunology.uzh.ch (B.B.), lukas.flatz@med.uni-tuebingen.de (L.F.)

https://doi.org/10.1016/j.medj.2022.12.007

Please cite this article in press as: Nuñez et al., Immune signatures predict development of autoimmune toxicity in patients with cancer treated with immune checkpoint inhibitors, Med (2023), https://doi.org/10.1016/j.medj.2022.12.007

CellPress
OPEN ACCESS

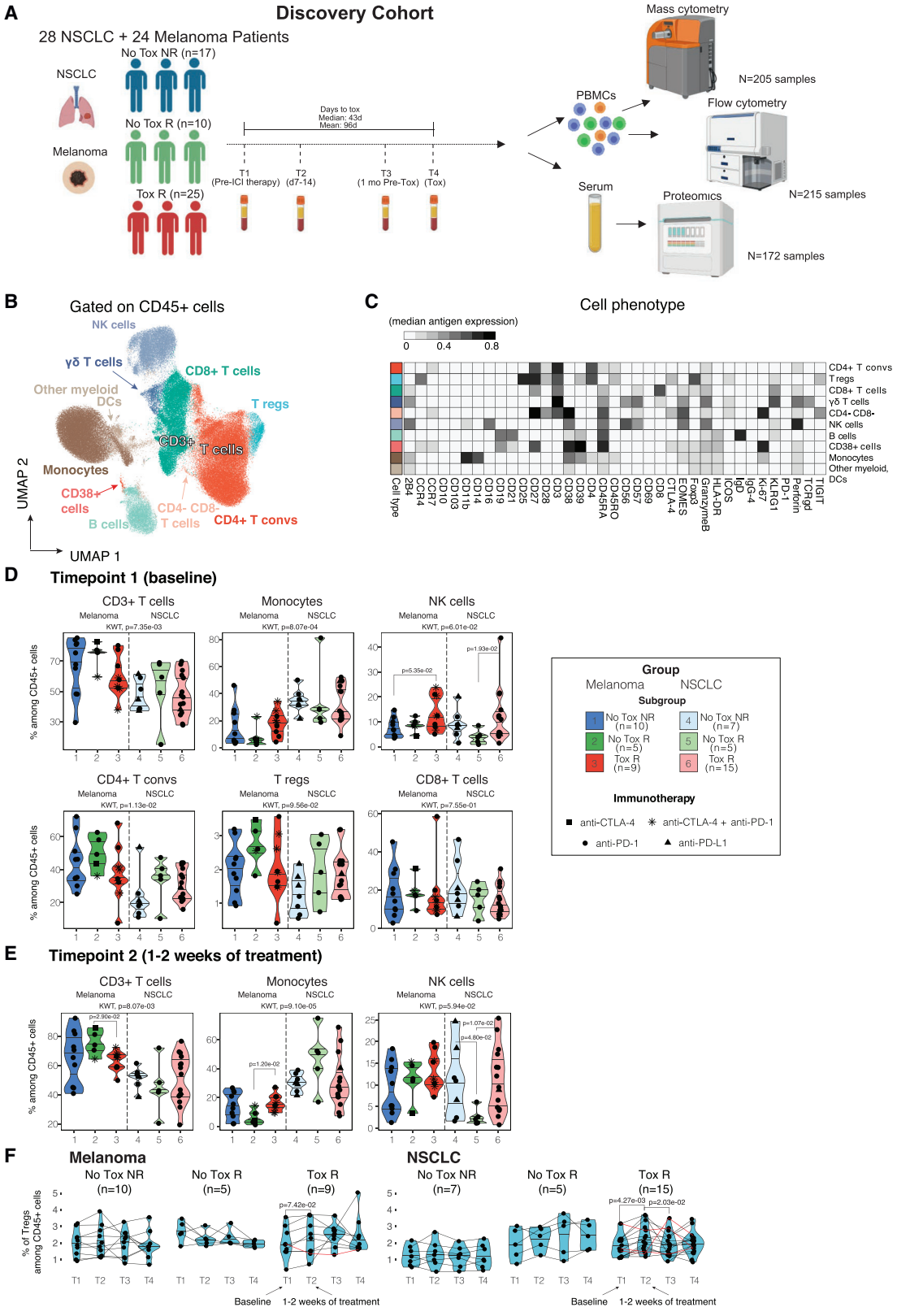

Please cite this article in press as: Nuñez et al., Immune signatures predict development of autoimmune toxicity in patients with cancer treated with immune checkpoint inhibitors, Med (2023), https://doi.org/10.1016/j.medj.2022.12.007

Figure 1. Frequencies of CD45$^+$ cells before therapy and over time in ICI-treated patients with melanoma or NSCLC

(A) Graphical representation of the experimental approach for the discovery cohort. Patients with NSCLC or melanoma were retrospectively divided into treatment responders with ICI toxicity (Tox Rs), no toxicity responders (No Tox Rs), and no tox non-responders (No Tox NRs). Cryo-preserved samples from four time points per patient were selected for analysis.

(B) Uniform manifold approximation and projection (UMAP) showing the FlowSOM-guided manual metaclustering of CD45$^+$ cells in PBMCs. Cells were proportionally combined from patients with melanoma and those with NSCLC at different time points to create the UMAP map.

(C) Heatmap showing the median intensity of marker expression (value range: 0–1) for the annotated CD45$^+$ subsets.

(D and E) Violin plots depict the frequencies of the indicated populations among total CD45$^+$ cells in the studied groups at T1 (pre-therapy) and T2 (1 to 2 weeks after the start of therapy). p values calculated using the Kruskal-Wallis test (KWT) indicate differences between the six groups of patients. Mann-Whitney-Wilcoxon test was performed to compare patients with the same cancer type (only statistically significant p values are displayed; $p < 0.05$).

(F) Violin plots show the frequency of Tregs among total CD45$^+$ cells over time in patients with and without toxicity. Lines that sloped down were plotted in red. Only statistically significant p values are displayed ($p < 0.05$, Mann-Whitney-Wilcoxon test, paired).

significantly better overall survival (OS) (melanoma: hazard ratio [HR] = 0.46 [95% confidence interval (CI), 0.20–1.1], p = 0.034; NSCLC: HR = 0.29 [95% CI, 0.18–0.47], $p < 0.0001$) (Figures S1E and S1F) and progression-free survival (PFS) (melanoma: HR = 0.53 [95% CI, 0.23–1.2], p = 0.084; NSCLC: HR = 0.28 [95% CI, 0.17–0.46], $p < 0.0001$) than those without (Figures S1G and S1H). These data confirmed previous findings showing that development of ICI-induced irAEs is associated with improved patient survival.

Canonical blood leukocyte frequencies pre-ICI therapy were similar between patients with the same type of cancer, independent of irAE development

We then asked whether we could detect any pre-treatment differences between the systemic immune compartments of patients who later went on to develop irAEs and those that did not. From our prospectively recruited patient cohort, we selected a representative discovery cohort consisting of patients for whom blood draws pre-therapy and throughout therapy were available. The discovery cohort consisted of three subgroups of patients with melanoma or NSCLC: patients with responding tumors who developed irAEs (Tox Rs, n = 25), patients with responding tumors who did not develop irAEs (No Tox Rs, n = 10), and patients with non-responding tumors who did not develop irAEs (No Tox NRs, n = 17) (Figure S1I; Table S1). The Tox NR subgroup (patients with non-responding tumors who developed irAEs) was excluded in the discovery cohort due to incomplete datasets. We analyzed over 200 cryopreserved samples of peripheral blood mononuclear cells (PBMCs) and 172 serum samples taken immediately before the start of ICI therapy (T1); we also collected samples for later analysis at 1 or 2 weeks after the start of ICI therapy (T2), at a time point corresponding to 1 month before the onset of the first irAE in affected patients (T3), and at the onset of the first irAE (T4). For patients without irAEs, we selected samples for T3 and T4 that corresponded as closely as possible to the timing of T3 and T4 of patients with irAEs (Figure 1A).

We first compared the frequencies of the main cell types present in PBMCs from patients with melanoma or NSCLC prior to the start of ICI treatment using high-parametric mass and flow cytometry to identify the major leukocyte (CD45$^+$) populations (Figures 1B and 1C). Within patient subgroups with the same cancer type, we found comparable levels of CD3$^+$ T cells, monocytes, CD4$^+$ conventional T cells (Tconvs), regulatory T cells (Tregs), and CD8$^+$ T cells (Figure 1D), as well as of CD4$^-$ CD8$^-$ T cells, γδT cells, B cells, CD38$^+$ cells, and other myeloid cells (Figure S1J). However, we did find differences between the two cancer types, including a higher frequency of CD3$^+$ T cells and a lower proportion of monocytes in patients with melanoma compared with those with NSCLC (Figure 1D). In addition, in the NSCLC group, we uncovered significantly higher frequencies of natural killer (NK) cells in NSCLC Tox R patients compared with No Tox R patients, as well as higher frequencies of NK cells in melanoma Tox R patients compared with No Tox NR patients (Figure 1D).

Please cite this article in press as: Nuñez et al., Immune signatures predict development of autoimmune toxicity in patients with cancer treated with immune checkpoint inhibitors, Med (2023), https://doi.org/10.1016/j.medj.2022.12.007

CellPress
OPEN ACCESS

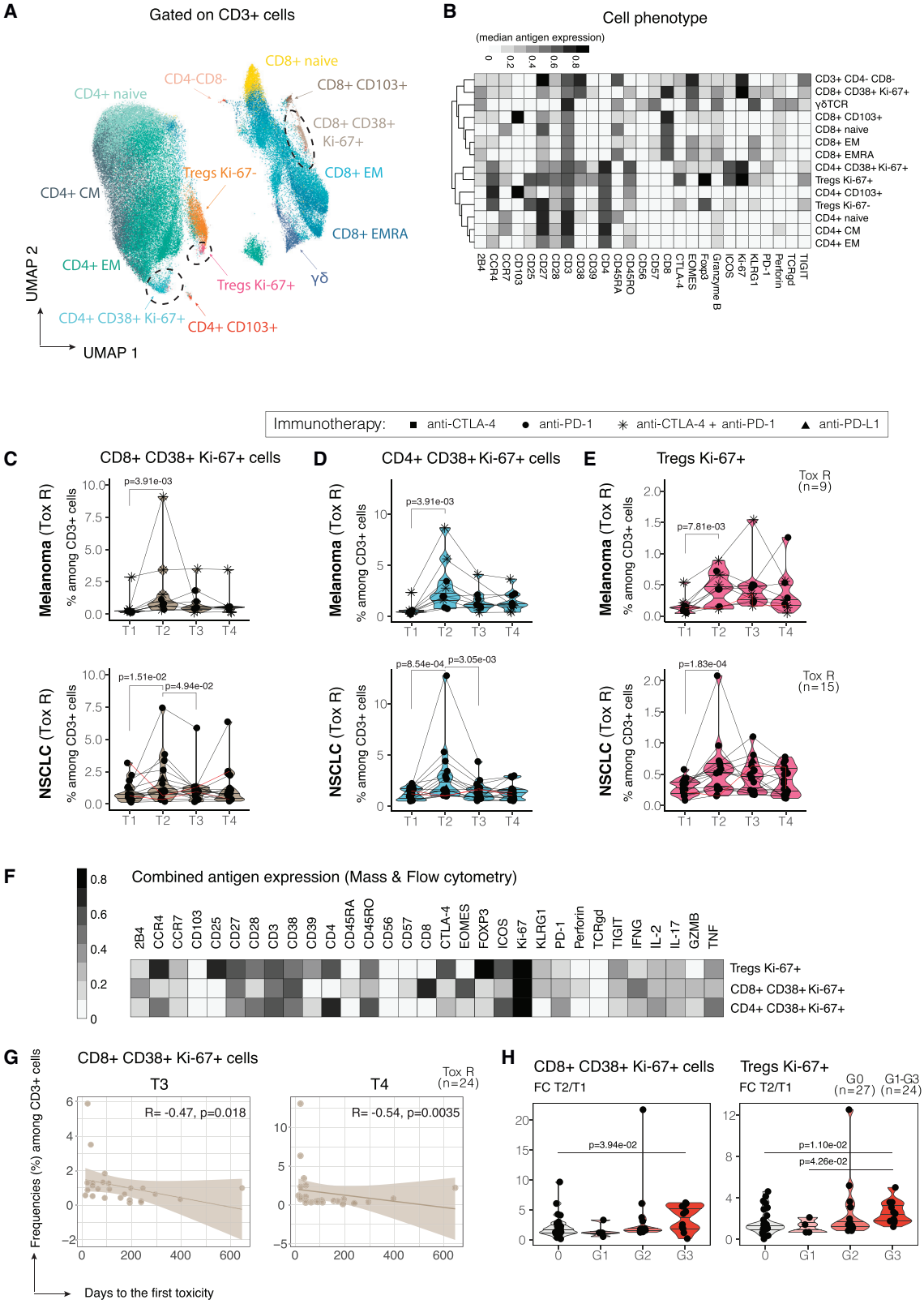

Please cite this article in press as: Nuñez et al., Immune signatures predict development of autoimmune toxicity in patients with cancer treated with immune checkpoint inhibitors, Med (2023), https://doi.org/10.1016/j.medj.2022.12.007

Figure 2. Expansion of proliferating (Ki-67$^+$) T cell subsets in patients with irAEs

(A) UMAP map showing the FlowSOM-guided manual metaclustering of CD3$^+$ cells in PBMCs. Cells were proportionally combined from patients with melanoma and those with NSCLC at different time points to create the UMAP map.

(B) Heatmap showing the median intensity of marker expression (value range: 0–1) for the annotated T cell subsets.

(C–E) Paired violin plots show the relative frequencies of the indicated cell populations before and during ICI treatment. Lines that sloped down were plotted in red. Only statistically significant p values are displayed ($p < 0.05$, Mann-Whitney-Wilcoxon test, paired).

(F) The heatmap summarizes the mass and flow cytometry results of some of the identified CD3$^+$ populations, showing their relative expression levels of activation markers and cytokines.

(G) Pearson correlation between the relative frequencies of Ki-67$^+$CD38$^+$CD8$^+$ cells among CD3$^+$ cells and days to the beginning of toxicity, showing that patients with higher frequencies of Ki-67$^+$CD38$^+$CD8$^+$ cells at T3 and T4 developed toxicity sooner after the first dose of ICI therapy.

(H) Violin plots showing the differences in fold change of cell population frequency between T2/T1 in the patient groups. 0, no toxicity; G, grade. Only statistically significant p values are displayed ($p < 0.05$, Mann-Whitney-Wilcoxon test, non-paired).

After the first 1 to 2 weeks of treatment, we saw that the patients with melanoma in the Tox R subgroup had significantly lower frequencies of CD3$^+$ T cells and higher frequencies of monocytes compared with those in the melanoma No Tox R subgroup (Figure 1E). We also found that the difference in frequencies of NK cells between NSCLC Tox Rs and No Tox Rs at T1 (Figure 1D) was preserved at T2 (Figure 1E). All other cell populations had comparable frequencies in Tox and No Tox subgroups at T2 (Figure S1K). Next, we extended our analysis to compare T1–T4 samples between patients with and without irAEs. We found that NSCLC Tox R patients exhibited a significant increase in relative frequency of Tregs 1 to 2 weeks after the start of therapy—a trend that we also found in melanoma Tox Rs. This was not observed in patients who did not develop irAEs, regardless of their future response to therapy. In patients with NSCLC, the frequency of Tregs then decreased from T2 to T3 (Figure 1F). As we observed most differences in the T cell compartment, and because T cells are the main target of ICIs, with their activity predicting response to ICI therapy,[20–23] hereafter, our cellular analyses focused on T cell subsets.

Patients with cancer treated with ICIs developing irAEs showed an early expansion of proliferating T cell subsets

Within the CD4$^+$ and CD8$^+$ T cell compartment of PBMC samples from patients with melanoma or NSCLC, we identified naive, central memory (CM), effector memory (EM), and terminally differentiated effector memory cells re-expressing CD45RA (EMRA) (Figure 2A). We also identified several subsets distinguished by their expression of CD103, as well as by their proliferative state, as assessed through CD38 and Ki-67 expression; lastly, we identified γδTCR and CD3$^+$CD4$^-$CD8$^-$ T cells (Figures 2A and 2B). We uncovered several significant changes occurring within the T cell subsets of the Tox and No Tox subgroups across time points (Figures S2A and S2B). Among these changes, the most striking were in proliferating (Ki-67$^+$) subsets, which significantly expanded mainly in the Tox R subgroups from T1 to T2 in patients with melanoma and NSCLC: the proliferating subpopulations included CD8$^+$ CD38$^+$ Ki-67$^+$ T cells (Figure 2C), CD4$^+$ CD38$^+$ Ki-67$^+$ Tconvs (Figure 2D), and Ki-67$^+$ Tregs (Figure 2E).

We next asked whether the expansion of proliferating T cell subsets differed in patients receiving monotherapy (anti-PD-1 alone) versus those receiving combination therapy (anti-CTLA4 + anti-PD1). Of note, for the combination treatment, the analysis could only be performed for Tox R subgroups as patients in the No Tox subgroups in our cohort were not treated with combined ICIs (Figure S2C). When analyzing the treatments individually, we could still observe an expansion of proliferating T cell subsets from T1 to T2 in the Tox R subgroups, although this specific stratification into smaller patient subgroups made robust statistical analysis challenging (Figures S2D and S2E). Taken together, these data showed that an early expansion of proliferating T cell subsets occurred in the Tox R subgroups during ICI therapy.

Please cite this article in press as: Nuñez et al., Immune signatures predict development of autoimmune toxicity in patients with cancer treated with immune checkpoint inhibitors, Med (2023), https://doi.org/10.1016/j.medj.2022.12.007

Patients with expanding CD8$^+$ CD38$^+$ Ki-67$^+$ T cells were more likely to develop irAEs early in their treatment

We next assessed the functionality of the T cells from the discovery cohort samples by activating them *ex vivo* with PMA/ionomycin and then detecting cytokine production by flow cytometry. Figure 2F shows the combined activation status and cytokine secretion profiles of these proliferating T cell subsets. CD4$^+$ CD38$^+$ Ki-67$^+$ T cells and Ki-67$^+$ Tregs expressed high levels of CCR4, ICOS, and CD28. CD8$^+$ CD38$^+$ Ki-67$^+$ T cells showed high intensities of 2B4, Eomes, and interferon-γ (IFN-γ).

When we looked at the relationship between days to the start of toxicity and the frequency of CD8$^+$ CD38$^+$ Ki-67$^+$ T cells, we found that patients with higher frequencies of these cells at T3 or T4 (time point of autoimmune toxicity) were likely to develop autoimmune toxicity sooner (Figure 2G), supporting the possible role of this T cell subset in the development of irAEs. We next analyzed the fold change in the frequency of proliferating T cell subsets among patients with different grades of irAEs from T1 to T2. We found that patients experiencing one or more grade 3 irAEs had a significantly higher relative increase from T1 to T2 in the frequency of CD8$^+$ CD38$^+$ Ki-67$^+$ cells and Ki-67$^+$ Tregs compared with patients not experiencing irAEs, as shown by the T2:T1 fold change. Patients experiencing grade 3 irAEs also had a significantly higher relative increase in Ki-67$^+$ Tregs from T1 to T2 compared with patients experiencing only grade 1 irAEs (Figure 2H). These data suggested that an early expansion of the identified proliferating T cell subsets is associated with the development of higher-grade irAEs.

Patients developing irAEs showed an early increase in the expression of proteins associated with the IFN-γ signaling pathway

Serum biomarkers are especially desirable as blood can be obtained easily with minimal discomfort to the patient, and serum analysis can be conducted rapidly, accurately, and inexpensively. Therefore, alongside our single-cell immunoprofiling, we measured the expression of 92 proteins (Olink inflammation panel) in 172 serum samples from the two patient groups of our discovery cohort. We found that pretherapy protein expression was markedly different between patients with melanoma and those with NSCLC (Figure S3A), but no significant differences were found among subgroups with and without irAEs at T1 in the two cancer types (see data and code availability in the STAR Methods). However, when we analyzed the protein expression kinetics, we found a significant increase in the expression of proteins associated with the IFN-γ signaling pathway in Tox R patients from T1 to T2 (just 1 to 2 weeks after the start of ICI therapy), including increases in CXCL9, CXCL10, CXCL11, FGF5, and IFN-γ (EnrichR; Table S2). We did not observe any significant increase in the expression of these proteins in the No Tox subgroups (Figures S3B and S3C). When we compared the fold change in expression of these proteins from T1 to T2 among the different subgroups, we found that in patients with melanoma, Tox Rs had a significantly higher relative increase in several of these proteins from T1 to T2 compared with both No Tox Rs and No Tox NRs (Figure S3D). This difference was not significant in patients with NSCLC (Figure S3E). In both cancer types, the serum proteins with the highest fold change in expression from T1 to T2 were CXCL9, CXCL10, CXCL11, and IFN-γ (Figures 3A and 3B).

To exclude that the observed differences were due to the type of ICI therapy, we also analyzed the expansion of these cytokines in patients with melanoma treated with monotherapy (anti-PD-1), and we again observed a significant expansion of cytokines from T1 to T2 in this stratified Tox R subgroup (Figure S3F). In the melanoma group, we also noted a broader increase in proteins from T1 to T2: the expression

Please cite this article in press as: Nuñez et al., Immune signatures predict development of autoimmune toxicity in patients with cancer treated with immune checkpoint inhibitors, Med (2023), https://doi.org/10.1016/j.medj.2022.12.007

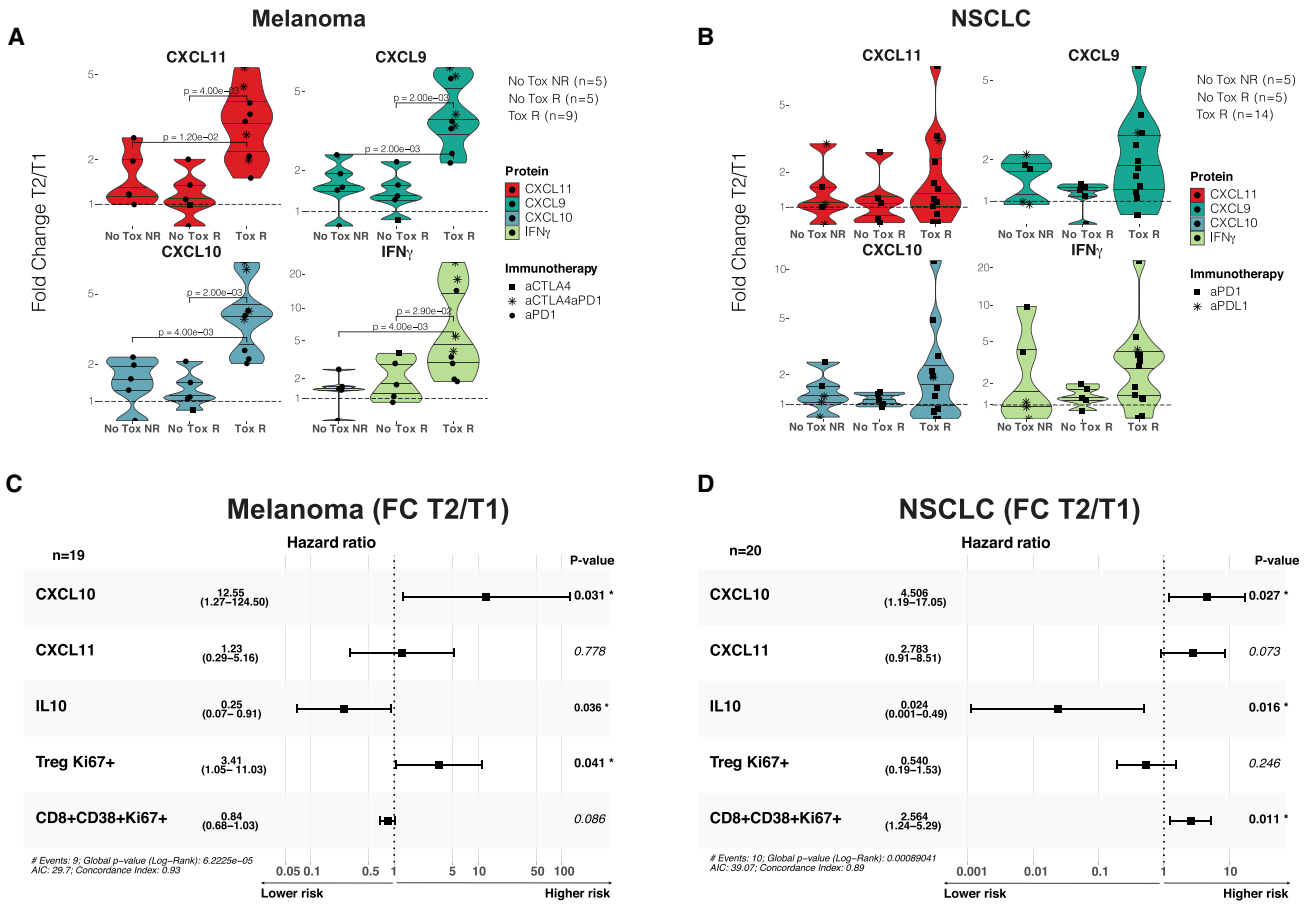

Figure 3. Serum proteomics and predictive biomarkers for autoimmune toxicity in ICI-treated patients with cancer (discovery cohort)

(A and B) Violin plots show the most significant differences in fold change between T1/T2 in the abundance of the analyzed serum proteins in patients with melanoma (A) or NSCLC (B). Only statistically significant p values are displayed ($p < 0.05$, Mann-Whitney-Wilcoxon test, non-paired).

(C and D) Multi-variate Cox regression analysis shows potential biomarkers of future autoimmune toxicity in patients with melanoma (C) and NSCLC (D).

of several cytokines (e.g., tumor necrosis factor [TNF], interleukin-18 [IL-18], IL-8, OSM, and IL-10) and chemokines (e.g., MCP3, MCP4, CCL3, CCL4, CX3CL1, CXCL6, CXCL10, and CCL19) markedly increased in the Tox R subgroup. These increases in protein levels from T1 to T2 were not observed in the melanoma No Tox subgroups (Figure S3G). These findings therefore demonstrated that the early increase in IFN-γ-related proteins in serum during ICI therapy was specifically associated with the Tox R subgroup.

A potential biomarker profile to predict the development of ICI-irAEs in patients with cancer

Next, to analyze the predictive value of the change in parameters obtained by cytometry and proteomics from T1 to T2, we employed logistic regression to create a receiver operating characteristic curve (ROC), which showed that the early expansion of IFN-γ-driven cytokines and of Ki-67$^+$ T cell subsets provided a good prediction model that allowed us to distinguish between patients who later developed irAEs and those that did not (Figures S3H and S3I). Then, to better understand the relationship between the parameters analyzed and the time to irAE onset, we used a Cox proportional-hazards (Coxph) model with which we identified several variables that could predict the later occurrence of ICI-induced irAEs: overall, patients exhibiting an early increase in expression of individual IFN-γ-driven cytokines

Please cite this article in press as: Nuñez et al., Immune signatures predict development of autoimmune toxicity in patients with cancer treated with immune checkpoint inhibitors, Med (2023), https://doi.org/10.1016/j.medj.2022.12.007

and proliferating T cell subsets were at significantly increased risk of developing irAEs early in treatment (Table S3). Moreover, in the multi-variable analysis, we found that an increase in serum CXCL10 from T1 to T2 was associated with higher risk of early development of irAEs in both the melanoma and NSCLC groups, while expansion of Ki-67$^+$ Tregs and CD8$^+$ Ki-67$^+$ CD38$^+$ T cells between T1 and T2 was significantly associated with higher risk of autoimmune toxicity in patients with melanoma and NSCLC, respectively. On the other hand, an increase in IL-10 levels between these time points was associated with reduced risk of irAE development (Figures 3C and 3D). We also found that pre-therapy and on-therapy frequencies in monocyte, NK cell, and B cell subsets, as well as in other proteins analyzed, were not associated with the development of autoimmune toxicity (Table S4).

To more clearly determine whether these signatures were specifically associated with irAEs or also with response to ICI therapy, we compared the fold change from T1 to T2 of serum proteins between Rs and NRs. In patients with melanoma, Rs had a significantly higher expansion of IL-17A and IFN-γ. However, none of the chemokines (including CXCL9, CXCL10, and CXCL11) found to be expanded in the Tox R subgroup were expanded in the R subgroup, showing that this chemokine signature was more likely associated with the development of irAEs (Figures S3J and S3D). Instead, in patients with NSCLC, the T1 to T2 fold change in serum proteins between Rs/NRs was similar to that observed between Tox R versus No Tox NR patients (Figures S3E and S3K). As above, we generated an ROC to determine whether the early expansion of IFN-γ-driven cytokines and Ki-67$^+$ T cell subsets found to be associated with autoimmune toxicity was also associated with response to ICI therapy. We found that patients with melanoma who had increasing levels of IFN-γ-driven cytokines and elevated frequencies of proliferating T cells were more likely to respond to ICI therapy, in line with previous studies[24,25] (Figure S3L). This shows that the immune signatures of response and autoimmune toxicity are likely to be at least in part overlapping; this was less apparent in patients with NSCLC (Figure S3M). When we used a Coxph model to analyze the predictive value of the parameters for response to ICI therapy, some were significant in the univariate analysis, although none of the significant parameters associated with response were also associated with autoimmune toxicity (Table S4). Similarly, in the multi-variable analysis, none of the parameters that were associated with the early development of irAEs were also associated with OS in ICI therapy in the melanoma or NSCLC groups (Figures S3N and S3O), showing that the immune signatures identified were more strongly associated with the development of irAEs than with response to ICI therapy. In summary, these data showed that the identified immune signatures occurring early during ICI therapy were more strongly associated with irAEs than with response to therapy, although they were partially overlapping.

Cytokine signatures were predictive of ICI-induced irAEs in patients with melanoma

To validate our biomarker findings and more clearly define the immune signatures relating to autoimmune toxicity versus response to ICI therapy, we used spectral multi-color flow cytometry and proteomics to analyze an independent multi-center validation cohort of ICI-treated patients with melanoma or NSCLC recruited from two centers in Switzerland and three centers in Germany. In this validation cohort, we were able to include a Tox NR subgroup (patients not responding to ICI therapy but developing irAEs), which was not available for the discovery cohort. The validation cohort consisted of 98 Tox R, 63 Tox NR, 43 No Tox R, and 33 No Tox NR patients (Table S1). We first analyzed the T cell subsets in 108 PBMC samples

Please cite this article in press as: Nuñez et al., Immune signatures predict development of autoimmune toxicity in patients with cancer treated with immune checkpoint inhibitors, Med (2023), https://doi.org/10.1016/j.medj.2022.12.007

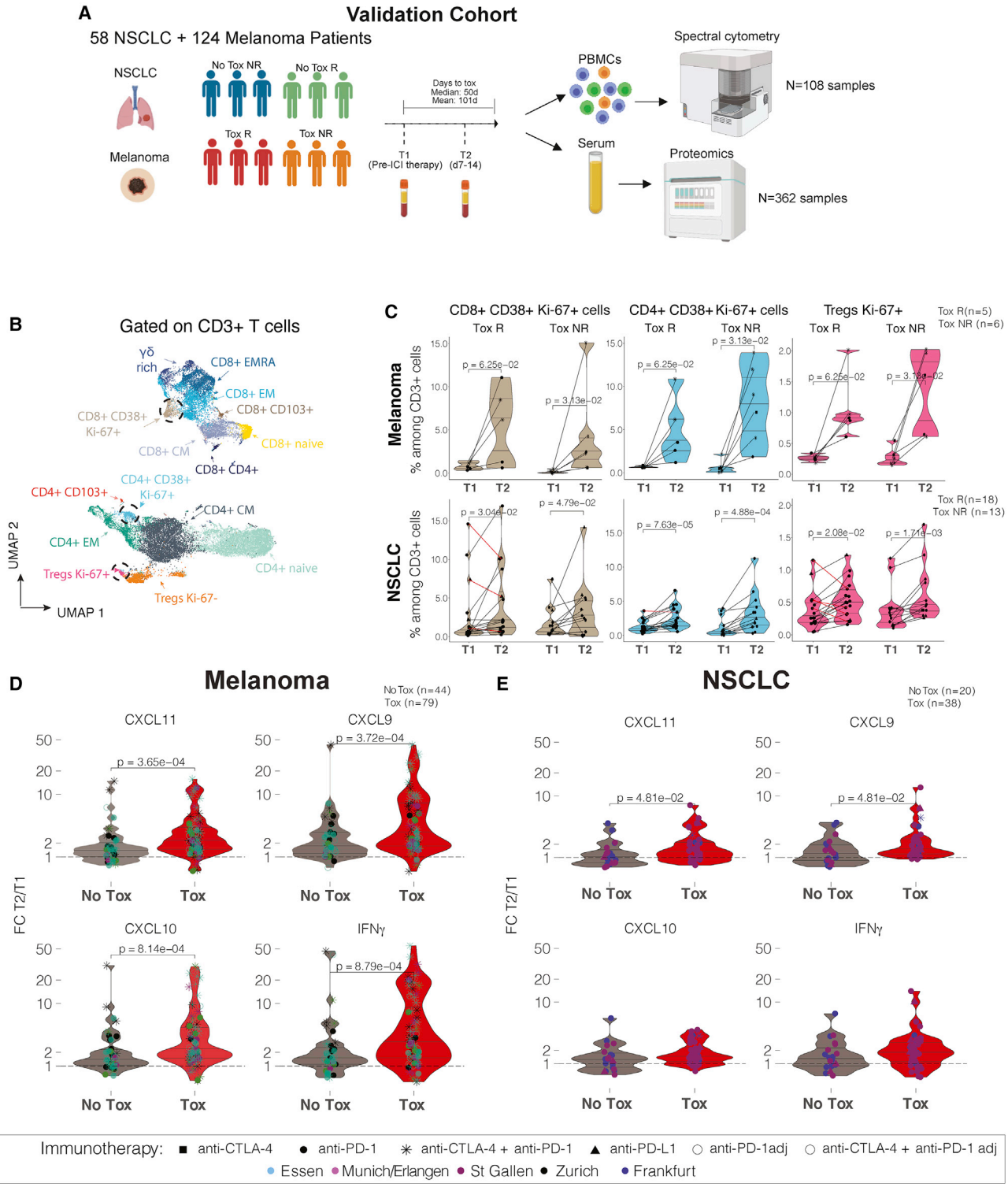

Figure 4. Spectral cytometry, serum proteomics, and predictive biomarkers for autoimmune toxicity in ICI-treated patients with cancer (validation cohort)

(A) Graphical representation of the experimental approach. Patients with NSCLC or melanoma were retrospectively divided into treatment responders with ICI toxicity (Tox Rs), no toxicity responders (No Tox Rs), no tox non-responders (No Tox NRs), and toxicity responders (Tox Rs). Cryo-preserved samples from two time points per patient were selected for analysis.

Please cite this article in press as: Nuñez et al., Immune signatures predict development of autoimmune toxicity in patients with cancer treated with immune checkpoint inhibitors, Med (2023), https://doi.org/10.1016/j.medj.2022.12.007

Figure 4. *Continued*

(B) UMAP map showing the FlowSOM-guided manual metaclustering of $CD3^+$ cells in PBMCs. Cells were proportionally combined from patients with melanoma and those with NSCLC at different time points to create the UMAP map.

(C) Paired violin plots show the relative frequencies of the indicated cell populations before and during ICI treatment. Lines that sloped down were plotted in red (Mann-Whitney-Wilcoxon test, paired).

(D and E) Violin plots showing the protein expansion in fold change from T1 to T2 in Tox and No Tox patients with melanoma (D) and NSCLC (E). Only statistically significant p values are displayed ($p < 0.05$, Mann-Whitney-Wilcoxon test, non-paired).

(Figure 4A). Figures 4B and S4A show the identified T cell populations that were compared among the different subgroups as well as their expression markers. As in the discovery cohort, we found that Tox R patients with melanoma and NSCLC had an expansion of $CD8^+$ $CD38^+$ Ki-67^+ T cells, $CD4^+$ $CD38^+$ Ki-67^+ T convs, and Ki-67^+ Tregs from T1 (pre-therapy) to T2 (1 to 2 weeks after start of therapy) (Figure 4C). Similarly, we detected a significant expansion in these T cell subsets at T2 in Tox NR patients but not in No Tox R or No Tox NR patients (Figures 4C and S4B), showing that the early expansion of these proliferating T cell subsets was associated with ICI-induced irAEs. Furthermore, we confirmed the previous proteomics findings by analyzing 362 additional serum samples (Figure S4C), showing that in melanoma Tox R and Tox NR subgroups, an early increase in CXCL9, CXCL10, CXCL11, and IFN-γ represented a signature predicting the later development of ICI-induced irAEs, independent of later response to ICI therapy (Figures 4D, S4D, and S4F). Although similar differences between Tox and No Tox patients were also observed in patients with NSCLC (Figures 4E, S4E, and S4G), additional validation would be required to confirm their predictive power in this subgroup. Overall, in this multi-center study, we analyzed over 500 serum samples and over 300 PBMC samples from 235 patients (Figure S4C). Our results gave important insights into the underlying immunological mechanisms of irAE-induced immune responses and provided the first evidence for a clinically feasible means by which to identify those patients most at risk of developing irAEs during treatment with ICIs.

DISCUSSION

irAEs pose significant clinical challenges in the management of patients with cancer who are being treated with ICIs.[26] Although the mechanisms leading to ICI-induced irAEs are not well understood, there are several hypotheses, including antigen mimicry between tumor- and self-antigens[27,28]; breach of self-tolerance; tissue damage due to cytokine dysregulation; off-target effects in organs bearing the targeted immune checkpoint; microbiome alterations[29]; and tumor neoantigenicity.[30] What remains largely unknown is which immune cell subsets and soluble mediators are responsible. Importantly, biomarkers to predict which patients are more likely to develop ICI-irAEs are lacking.

In this study we combined clinical data with multi-parameter flow and mass cytometry (CyTOF) and serum proteomics to search for immune signatures that preceded the development of irAEs in ICI-treated patients with cancer. The most striking differences were observed at the early time points, specifically from baseline (pre-therapy) to 1 to 2 weeks after the start of treatment. Analyzing these samples, we identified dynamic changes occurring in the blood shortly after the initiation of ICI therapy that were significantly associated with the later development of irAEs, and these were found most strongly in patients with melanoma. In line with previous data in patients with melanoma and lung cancer whose tumors respond well to ICI therapy,[24,25] we found an increase in the frequency of proliferating Ki-67^+ $CD8^+$ $CD38^+$ and $CD4^+$ $CD38^+$ T cells shortly after starting ICI therapy, as well as of expanding Ki-67^+ Tregs, in patients later developing irAEs. Although Tregs suppress inflammation and autoimmunity and are thought to be primarily

Please cite this article in press as: Nuñez et al., Immune signatures predict development of autoimmune toxicity in patients with cancer treated with immune checkpoint inhibitors, Med (2023), https://doi.org/10.1016/j.medj.2022.12.007

pro-tumorigenic,[31,32] it is likely that Treg expansion follows the general immune activation induced by ICIs in patients who develop irAEs and whose tumors often respond well to therapy.[33] Despite the differences in the time taken for individual patients to manifest their first irAE, our findings suggest that it is these early immune changes in the first 1 to 2 weeks of therapy that are linked to whether or not patients will eventually experience ICI-related toxicity. The differences observed in the time to AE therefore do not affect the main conclusions.

Importantly, when we combined the parameters obtained from the multi-omics profiling of our discovery and validation cohorts, we were able to identify potential predictive biomarkers for ICI-induced irAEs. We propose that the analysis of serum proteins combined with the detection of proliferating T cell subsets 1 to 2 weeks after the start of therapy can help identify those patients at higher risk of later ICI toxicity: specifically, increased CXCL9 and CXCL10 and reduced IL-10 shortly after the start of therapy are likely indicators of heightened risk of developing irAEs. Serum biomarkers are particularly interesting in the clinical setting, and a recent study has shown the relevance of early proteomic changes in ICI-treated patients.[34] In addition, an early expansion of Ki-67$^+$ Tregs and Ki-67$^+$ CD8$^+$ T cells is also likely to be associated with increased risk of irAEs. Interestingly, while similar trends were seen in patients with melanoma and those with NSCLC, these biomarkers were more strongly associated with the development of irAEs in melanoma and require further investigation and validation in NSCLC.

A key aim of this study was to begin to distinguish immune signatures that are related to response to therapy versus those that predict toxicity. Indeed, it is well known that patients developing irAEs are more likely to respond well to therapy,[9] and here, too, we see evidence of a partial overlap of response- and irAE-related markers. However, we found that the early expansion of proliferating T cell subsets and the early increase in IFN-γ-related proteins were more strongly associated with autoimmune toxicity than with response to ICI therapy. CXCL9 and CXCL10 are produced by several cell types in response to IFN-γ and regulate immune cell migration, differentiation, and activation[35] and are known to be required for anti-tumor immune responses during ICI treatment.[36] Here, we see that the early increase in such serum proteins that are associated with the IFN-γ signaling pathway in patients with irAEs may be linked to the expansion of Ki-67$^+$ CD8$^+$ T cells, which abundantly express the CXCL9/CXCL10 receptor known as CXCR3.[37] Likewise, the reduction in IL-10 may also be associated with a proliferative CD8$^+$ T cell phenotype. Indeed, IL-10 is an anti-inflammatory cytokine that suppresses T cell activation[38] and was shown to inhibit proliferation and survival of IL-10R+ tumor-associated CD8$^+$ T cells in patients with melanoma.[39] In addition, one other study found that a decrease in IL-10 in patients with melanoma treated with anti-CTLA-4 was associated with irAEs.[40] Although we found that patients with irAEs had higher pre-therapy frequencies of NK cells, changes in NK cells during therapy were not associated with the development of autoimmune toxicity.

Overall, these findings show that while neither changes in T cell subsets nor serum biomarkers alone are sufficient to predict either response or toxicity during ICI therapy, combining these two information streams represents a powerful risk-assessment tool for early identification of those patients at highest risk of irAEs. While the identification of early on-treatment immunological markers may not prevent the development of irAEs, as the occurrence of autoimmune toxicity is often associated with tumor responsiveness, the primary aim should rather be to

improve patient care by allowing more effective monitoring and timely intervention with effective and life-saving management strategies. Further studies will be required to better dissect the immune signatures in patients whose tumors are responsive in the absence of irAEs and those in which the autoimmune toxicity comes hand in hand with tumor response. In summary, these findings shed light on the pathomechanisms of irAEs and identify candidate biomarkers for ICI-irAEs that may help to monitor patients at higher risk of developing such autoimmune toxicities.

Limitations of the study

The main limitation was the heterogeneity of the cohort, which included patients with different ICI treatments (monotherapy and combination therapy) and different ICI-induced irAEs. In particular, most patients without irAEs were treated with monotherapy, while patients with irAEs were treated with monotherapy or combination therapy. We performed subgroup analyses to take this into account; however, subdividing these smaller groups of patients made robust statistical analysis challenging, and further studies are needed to dissect this point completely. In addition, patients developed different numbers of irAEs and at different time points. Although most irAEs occurred within a median time of around 40 days from the start of ICI treatment, the interval of irAE development varied among patients (Table S1), making predicting the timing of emergence of toxicity impossible. However, the advantage of our experimental design is that by focusing on early time points, the later heterogeneity of the cohort that later emerged does not represent a confounding factor for our analyses and did not prevent us from identifying predictors of irAEs. A second limitation was the relatively low patient number in some of the patient subgroups, mainly the No Tox R subgroup; this is mainly due to the clinical reality that the majority of patients who respond to ICI therapy experience some form of irAEs. A third limitation was related to the finding that the identified immune signatures, while being more strongly associated with ICI-induced irAEs, were also associated with response to ICI therapy, although we were able to go some way toward dissecting these effects.

STAR★METHODS

Detailed methods are provided in the online version of this paper and include the following:

- KEY RESOURCES TABLE
- RESOURCE AVAILABILITY
  - Lead contact
  - Materials availability
  - Data and code availability
- EXPERIMENTAL MODEL AND SUBJECT DETAILS
- METHOD DETAILS
  - Clinical samples
  - *Ex vivo* reactivation of PBMCs
  - Cell stimulation and flow cytometry data acquisition
  - Cellular barcoding and mass cytometry acquisition
  - High-dimensional flow cytometry and mass cytometry analysis
  - Proteomics
- QUANTIFICATION AND STATISTICAL ANALYSIS

SUPPLEMENTAL INFORMATION

Supplemental information can be found online at https://doi.org/10.1016/j.medj.2022.12.007.

Please cite this article in press as: Nuñez et al., Immune signatures predict development of autoimmune toxicity in patients with cancer treated with immune checkpoint inhibitors, Med (2023), https://doi.org/10.1016/j.medj.2022.12.007

ACKNOWLEDGMENTS

We thank Dr. T. Wertheirmer, C. Merten, and A. Sethi for technical support. We thank Dr. Lucy Robinson from Insight Editing London for critical review and editing of the manuscript. The graphical abstract was created with BioRender.com. We greatly thank the patients who contributed to this study. This project has received funding from the European Research Council (ERC) under the European Union's Horizon 2020 research and innovation program grant agreement no. 882424 and the Swiss National Science Foundation (733 310030_170320, 310030_188450, CRSII5_183478 to B.B., and PP00P3_187189 to L.F.). N.G.N. is a recipient of a University Research Priority Program (URPP) postdoctoral fellowship. S.K. is a recipient of a research fellowship from the German Research Foundation (DFG). In addition, this project received funding from the Swiss Cancer League (KLS-4409-02-2018), the Forschungsförderung of the Kantonsspital St.Gallen, Hookipa Pharma, and the Novartis Foundation.

AUTHOR CONTRIBUTIONS

Experimental design, N.G.N., E.F., S.U., F.B., B.B., and L.F.; data acquisition and analysis, N.G.N., E.F., S.U., F.B., W.v.d.V., L.C., A.H., and D.B.; data interpretation, N.G.N., E.F., and F.B.; sample and patient data collection and processing, F.B., L.F., N.W., M.-T.P., R.N., M.P., C.L., O.H.A., S.D., M.-T.A., M.P.L., J.M.G., P.A.A., M.C., G.M., T.A., R.D., R.K., M.E., C.S., L.H., E.J., J.K., D.S., L.Z., S.U., N.K., and M.H.; data analysis, N.G.N., E.F., and F.B.; manuscript writing, F.B., N.G.N., E.F., B.B., and L.F.; critical revision of the manuscript, B.B. and L.F.; clinical information, F.B., L.F., N.W., J.M.G., M.C., R.K., M.E., C.S., L.H., E.J., J.K., D.S., L.Z., S.U., N.K., M.H., M.J., and M.F.; technical or material support, M.-T.A., S.K., L.P., A.H., F.D., C.D., M.J., and M.F.; funding and study supervision, B.B. and L.F.

DECLARATION OF INTERESTS

L.F. has/had advisory roles for Novartis, Sanofi, Philogen, and Bristol-Myers Squibb, all which took place outside the submitted work. P.A.A. has/had consultant/advisory roles for Bristol-Myers Squibb, Roche-Genentech, Merck Sharp & Dohme, Novartis, Array BioPharma, Merck Serono, Pierre Fabre, Incyte, MedImmune, AstraZeneca, Syndax, Sun Pharma, Sanofi, Idera, Ultimovacs, Sandoz, Immunocore, 4SC, Alkermes, Italfarmaco, Nektar, Boehringer-Ingelheim, Eisai, Regeneron, Daiichi Sankyo, Pfizer, Oncosec, Nouscom, Takis, Lunaphore Technologies, Seattle Genetics, ITeos Therapeutics, Medicenna, Bio-Al Health, and ValoTx; he also received research funding from Bristol-Myers Squibb, Roche-Genentech, Array, Sanofi, and Pfizer, as well as travel support from Merck Sharp & Dhome and Pfizer, all which was outside the submitted work. T.A. served as consultant to Bristol-Myers Squibb, Novartis, and CeCaVa; received travel support from Bristol-Myers Squibb and Novartis; received speaker fees from Novartis, Bristol-Myers Squibb, Pierre Fabre, and CeCaVa; received institutional funding from Neracare, Novartis, Sanofi, and SkylineDX; and received institutional research grants from Novartis outside the submitted work. R.D. has intermittent, project-focused consulting and/or advisory relationships with Novartis, Merck Sharp & Dhome, Bristol-Myers Squibb, Roche, Amgen, Takeda, Pierre Fabre, Sun Pharma, Sanofi, Catalym, Second Genome, Regeneron, Alligator, T3 Pharma, MaxiVAX SA, Pfizer, and touchIME, all which took place outside the submitted work. W.v.d.V. declares research support from the Novartis research foundation and the PROMEDICA Stiftung and serves as a consultant for Mabylon outside the submitted work. S.U. declares research support from Bristol-Myers Squibb and Merck Serono; speakers and advisory board honoraria from Bristol-Myers Squibb, Merck Sharp & Dohme, Merck Serono, Novartis, and

Roche; and travel support from Bristol-Myers Squibb, Merck Sharp & Dohme, and Pierre Fabre outside the submitted work. L.Z. declares speakers and advisory board honoraria from Bristol-Myers Squibb, Merck Sharp & Dohme, Novartis, Pierre Fabre, Sanofi, and Sunpharma; research support from Novartis; and travel support from Merck Sharp & Dohme, Bristol-Myers Squibb, Pierre Fabre, Sanofi, Sunpharma, and Novartis outside the submitted work. F.D. receives/received honoraria and travel support from Merck Sharp & Dohme, Bristol-Myers Squibb, and Sun Pharma outside the submitted work. L.H. declares research support from Therakos and speakers and advisory board honoraria from Amgen, BiomeDx, Bristol-Myers Squibb, Curevac, Merck, Merck Sharp & Dohme, Myoncare, Novartis, Pierre Fabre, Sanofi, SUN, and Roche, outside the submitted work. M.E. declares honoraria and travel support from Bristol-Myers Squibb, Immunocore, and Novartis outside the submitted work. R.K. declares travel support from Pierre Fabre and Sun Pharma outside the submitted work. M.J. declares advisory roles (institutional) for Novartis, AstraZeneca, Basilea Pharmaceutica, Bayer, Bristol-Myers Squibb, Debiopharm, Merck Sharp & Dhome, Roche, and Sanofi; research funding from Swiss Cancer Research; and travel grants from Roche, Sanofi, and Takeda. D.S. has/had consultant/advisory roles in the last 3 years for Bristol-Myers Squibb, Merck Sharp & Dohme, Novartis, Array, Merck Serono, Pfizer, Pierre Fabre, Sun Pharma, Sanofi, Regeneron, Ultimovacs, Sandoz, Immunocore, 4SC, Neracare, Nektar, Daiichi Sankyo, Oncosec, Amgen, BioCon, Immatics, InFlarX, Innovent, Labcorp, Replimune, and Haystack; his institution also received research funding from Bristol-Myers Squibb, Roche-Genentech, Array, and Merck Sharp & Dhome, all of which took place outside the submitted work. N.K. received personal fees, travel costs, and speaker's honoraria from Astellas, Novartis, Ipsen, and Photocure, all of which took place outside the submitted work. M.P.L. has received project-specific research funding from Roche, Novartis, Molecular Partners, and Oncobit.

INCLUSION AND DIVERSITY

We support inclusive, diverse, and equitable conduct of research.

Received: November 29, 2022
Revised: December 16, 2022
Accepted: December 21, 2022
Published: January 23, 2023

REFERENCES

1. Robert, C., Long, G.V., Brady, B., Dutriaux, C., Maio, M., Mortier, L., Hassel, J.C., Rutkowski, P., McNeil, C., Kalinka-Warzocha, E., et al. (2015). Nivolumab in previously untreated melanoma without BRAF mutation. N. Engl. J. Med. *372*, 320–330. https://doi.org/10.1056/NEJMoa1412082.

2. Larkin, J., Chiarion-Sileni, V., Gonzalez, R., Grob, J.J., Cowey, C.L., Lao, C.D., Schadendorf, D., Dummer, R., Smylie, M., Rutkowski, P., et al. (2015). Combined nivolumab and ipilimumab or monotherapy in untreated melanoma. N. Engl. J. Med. *373*, 23–34. https://doi.org/10.1056/NEJMoa1504030.

3. Borghaei, H., Paz-Ares, L., Horn, L., Spigel, D.R., Steins, M., Ready, N.E., Chow, L.Q., Vokes, E.E., Felip, E., Holgado, E., et al. (2015). Nivolumab versus docetaxel in advanced nonsquamous non-small-cell lung cancer. N. Engl. J. Med. *373*, 1627–1639. https://doi.org/10.1056/NEJMoa1507643.

4. Carbone, D.P., Reck, M., Paz-Ares, L., Creelan, B., Horn, L., Steins, M., Felip, E., van den Heuvel, M.M., Ciuleanu, T.E., Badin, F., et al. (2017). First-line nivolumab in stage IV or recurrent non-small-cell lung cancer. N. Engl. J. Med. *376*, 2415–2426. https://doi.org/10.1056/NEJMoa1613493.

5. Ribas, A., Puzanov, I., Dummer, R., Schadendorf, D., Hamid, O., Robert, C., Hodi, F.S., Schachter, J., Pavlick, A.C., Lewis, K.D., et al. (2015). Pembrolizumab versus investigator-choice chemotherapy for ipilimumab-refractory melanoma (KEYNOTE-002): a randomised, controlled, phase 2 trial. Lancet Oncol. *16*, 908–918. https://doi.org/10.1016/s1470-2045(15)00083-2.

6. Brahmer, J., Reckamp, K.L., Baas, P., Crinò, L., Eberhardt, W.E.E., Poddubskaya, E., Antonia, S., Pluzanski, A., Vokes, E.E., Holgado, E., et al. (2015). Nivolumab versus docetaxel in advanced squamous-cell non-small-cell lung cancer. N. Engl. J. Med. *373*, 123–135. https://doi.org/10.1056/NEJMoa1504627.

7. Reck, M., Rodríguez-Abreu, D., Robinson, A.G., Hui, R., Csőszi, T., Fülöp, A., Gottfried, M., Peled, N., Tafreshi, A., Cuffe, S., et al. (2016). Pembrolizumab versus chemotherapy for PD-L1-positive non-small-cell lung cancer. N. Engl. J. Med. *375*, 1823–1833. https://doi.org/10.1056/NEJMoa1606774.

8. Ellithi, M., Elnair, R., Chang, G.V., and Abdallah, M.A. (2020). Toxicities of immune checkpoint inhibitors: itis-ending adverse reactions and more. Cureus *12*, e6935. https://doi.org/10.7759/cureus.6935.

9. Petrelli, F., Grizzi, G., Ghidini, M., Ghidini, A., Ratti, M., Panni, S., Cabiddu, M., Ghilardi, M., Borgonovo, K., Parati, M.C., et al. (2020).

Immune-related adverse events and survival in solid tumors treated with immune checkpoint inhibitors: a systematic review and meta-analysis. J. Immunother. *43*, 1–7. https://doi.org/10.1097/CJI.0000000000000300.

10. Khan, S., and Gerber, D.E. (2020). Autoimmunity, checkpoint inhibitor therapy and immune-related adverse events: a review. Semin. Cancer Biol. *64*, 93–101. https://doi.org/10.1016/j.semcancer.2019.06.012.

11. Postow, M.A., Sidlow, R., and Hellmann, M.D. (2018). Immune-related adverse events associated with immune checkpoint blockade. N. Engl. J. Med. *378*, 158–168. https://doi.org/10.1056/NEJMra1703481.

12. Wang, D.Y., Salem, J.E., Cohen, J.V., Chandra, S., Menzer, C., Ye, F., Zhao, S., Das, S., Beckermann, K.E., Ha, L., et al. (2018). Fatal toxic effects associated with immune checkpoint inhibitors: a systematic review and meta-analysis. JAMA Oncol. *4*, 1721–1728. https://doi.org/10.1001/jamaoncol.2018.3923.

13. Weinmann, S.C., and Pisetsky, D.S. (2019). Mechanisms of immune-related adverse events during the treatment of cancer with immune checkpoint inhibitors. Rheumatology *58*, vii59–vii67. https://doi.org/10.1093/rheumatology/kez308.

14. Lim, S.Y., Lee, J.H., Gide, T.N., Menzies, A.M., Guminski, A., Carlino, M.S., Breen, E.J., Yang, J.Y.H., Ghazanfar, S., Kefford, R.F., et al. (2019). Circulating cytokines predict immune-related toxicity in melanoma patients receiving anti-PD-1-based immunotherapy. Clin. Cancer Res. *25*, 1557–1563. https://doi.org/10.1158/1078-0432.CCR-18-2795.

15. Lozano, A.X., Chaudhuri, A.A., Nene, A., Bacchiocchi, A., Earland, N., Vesely, M.D., Usmani, A., Turner, B.E., Steen, C.B., Luca, B.A., et al. (2022). T cell characteristics associated with toxicity to immune checkpoint blockade in patients with melanoma. Nat. Med. *28*, 353–362. https://doi.org/10.1038/s41591-021-01623-z.

16. Patil, P.D., Burotto, M., and Velcheti, V. (2018). Biomarkers for immune-related toxicities of checkpoint inhibitors: current progress and the road ahead. Expert Rev. Mol. Diagn. *18*, 297–305. https://doi.org/10.1080/14737159.2018.1440209.

17. Jia, X.H., Geng, L.Y., Jiang, P.P., Xu, H., Nan, K.J., Yao, Y., Jiang, L.L., Sun, H., Qin, T.J., and Guo, H. (2020). The biomarkers related to immune related adverse events caused by immune checkpoint inhibitors. J. Exp. Clin. Cancer Res. *39*, 284. https://doi.org/10.1186/s13046-020-01749-x.

18. Freeman-Keller, M., Kim, Y., Cronin, H., Richards, A., Gibney, G., and Weber, J.S. (2016). Nivolumab in resected and unresectable metastatic melanoma: characteristics of immune-related adverse events and association with outcomes. Clin. Cancer Res. *22*, 886–894. https://doi.org/10.1158/1078-0432.CCR-15-1136.

19. Haratani, K., Hayashi, H., Chiba, Y., Kudo, K., Yonesaka, K., Kato, R., Kaneda, H., Hasegawa, Y., Tanaka, K., Takeda, M., and Nakagawa, K. (2018). Association of immune-related adverse events with nivolumab efficacy in non-small-cell lung cancer. JAMA Oncol. *4*, 374–378. https://doi.org/10.1001/jamaoncol.2017.2925.

20. Huang, A.C., Postow, M.A., Orlowski, R.J., Mick, R., Bengsch, B., Manne, S., Xu, W., Harmon, S., Giles, J.R., Wenz, B., et al. (2017). T-cell invigoration to tumour burden ratio associated with anti-PD-1 response. Nature *545*, 60–65. https://doi.org/10.1038/nature22079.

21. Kamphorst, A.O., Pillai, R.N., Yang, S., Nasti, T.H., Akondy, R.S., Wieland, A., Sica, G.L., Yu, K., Koenig, L., Patel, N.T., et al. (2017). Proliferation of PD-1+ CD8 T cells in peripheral blood after PD-1-targeted therapy in lung cancer patients. Proc. Natl. Acad. Sci. USA *114*, 4993–4998. https://doi.org/10.1073/pnas.1705327114.

22. Gide, T.N., Quek, C., Menzies, A.M., Tasker, A.T., Shang, P., Holst, J., Madore, J., Lim, S.Y., Velickovic, R., Wongchenko, M., et al. (2019). Distinct immune cell populations define response to anti-PD-1 monotherapy and anti-PD-1/anti-CTLA-4 combined therapy. Cancer Cell *35*, 238–255.e6. https://doi.org/10.1016/j.ccell.2019.01.003.

23. Tumeh, P.C., Harview, C.L., Yearley, J.H., Shintaku, I.P., Taylor, E.J.M., Robert, L., Chmielowski, B., Spasic, M., Henry, G., Ciobanu, V., et al. (2014). PD-1 blockade induces responses by inhibiting adaptive immune resistance. Nature *515*, 568–571. https://doi.org/10.1038/nature13954.

24. Huang, A.C., Orlowski, R.J., Xu, X., Mick, R., George, S.M., Yan, P.K., Manne, S., Kraya, A.A., Wubbenhorst, B., Dorfman, L., et al. (2019). A single dose of neoadjuvant PD-1 blockade predicts clinical outcomes in resectable melanoma. Nat. Med. *25*, 454–461. https://doi.org/10.1038/s41591-019-0357-y.

25. Kim, K.H., Cho, J., Ku, B.M., Koh, J., Sun, J.M., Lee, S.H., Ahn, J.S., Cheon, J., Min, Y.J., Park, S.H., et al. (2019). The first-week proliferative response of peripheral blood PD-1(+)CD8(+) T cells predicts the response to anti-PD-1 therapy in solid tumors. Clin. Cancer Res. *25*, 2144–2154. https://doi.org/10.1158/1078-0432.CCR-18-1449.

26. Liu, Y.H., Zang, X.Y., Wang, J.C., Huang, S.S., Xu, J., and Zhang, P. (2019). Diagnosis and management of immune related adverse events (irAEs) in cancer immunotherapy. Biomed. Pharmacother. *120*, 109437. https://doi.org/10.1016/j.biopha.2019.109437.

27. Berner, F., Bomze, D., Diem, S., Ali, O.H., Fässler, M., Ring, S., Niederer, R., Ackermann, C.J., Baumgaertner, P., Pikor, N., et al. (2019). Association of checkpoint inhibitor-induced toxic effects with shared cancer and tissue antigens in non-small cell lung cancer. JAMA Oncol. *5*, 1043–1047. https://doi.org/10.1001/jamaoncol.2019.0402.

28. Berner, F., Bomze, D., Lichtensteiger, C., Walter, V., Niederer, R., Hasan Ali, O., Wyss, N., Bauer, J., Freudenmann, L.K., Marcu, A., et al. (2022). Autoreactive napsin A-specific T cells are enriched in lung tumors and inflammatory lung lesions during immune checkpoint blockade. Sci. Immunol. *7*, eabn9644. https://doi.org/10.1126/sciimmunol.abn9644.

29. Ramos-Casals, M., Brahmer, J.R., Callahan, M.K., Flores-Chávez, A., Keegan, N., Khamashta, M.A., Lambotte, O., Mariette, X., Prat, A., and Suárez-Almazor, M.E. (2020). Immune-related adverse events of checkpoint inhibitors. Nat. Rev. Dis. Prim. *6*, 38. https://doi.org/10.1038/s41572-020-0160-6.

30. Bomze, D., Hasan Ali, O., Bate, A., and Flatz, L. (2019). Association between immune-related adverse events during anti–PD-1 therapy and tumor mutational burden. JAMA Oncol. *5*, 1633–1635. https://doi.org/10.1001/jamaoncol.2019.3221.

31. Tanaka, A., and Sakaguchi, S. (2017). Regulatory T cells in cancer immunotherapy. Cell Res. *27*, 109–118. https://doi.org/10.1038/cr.2016.151.

32. Togashi, Y., Shitara, K., and Nishikawa, H. (2019). Regulatory T cells in cancer immunosuppression - implications for anticancer therapy. Nat. Rev. Clin. Oncol. *16*, 356–371. https://doi.org/10.1038/s41571-019-0175-7.

33. Koh, J., Hur, J.Y., Lee, K.Y., Kim, M.S., Heo, J.Y., Ku, B.M., Sun, J.M., Lee, S.H., Ahn, J.S., Park, K., and Ahn, M.J. (2020). Regulatory (FoxP3(+)) T cells and TGF-beta predict the response to anti-PD-1 immunotherapy in patients with non-small cell lung cancer. Sci. Rep. *10*, 18994. https://doi.org/10.1038/s41598-020-76130-1.

34. Klümper, N., Saal, J., Berner, F., Lichtensteiger, C., Wyss, N., Heine, A., Bauernfeind, F.G., Ellinger, J., Brossart, P., Diem, S., et al. (2022). C reactive protein flare predicts response to checkpoint inhibitor treatment in non-small cell lung cancer. J. Immunother. Cancer *10*, e004024. https://doi.org/10.1136/jitc-2021-004024.

35. Tokunaga, R., Zhang, W., Naseem, M., Puccini, A., Berger, M.D., Soni, S., McSkane, M., Baba, H., and Lenz, H.J. (2018). CXCL9, CXCL10, CXCL11/CXCR3 axis for immune activation - a target for novel cancer therapy. Cancer Treat Rev. *63*, 40–47. https://doi.org/10.1016/j.ctrv.2017.11.007.

36. House, I.G., Savas, P., Lai, J., Chen, A.X.Y., Oliver, A.J., Teo, Z.L., Todd, K.L., Henderson, M.A., Giuffrida, L., Petley, E.V., et al. (2020). Macrophage-derived CXCL9 and CXCL10 are required for antitumor immune responses following immune checkpoint blockade. Clin. Cancer Res. *26*, 487–504. https://doi.org/10.1158/1078-0432.CCR-19-1868.

37. Karin, N., and Razon, H. (2018). Chemokines beyond chemo-attraction: CXCL10 and its significant role in cancer and autoimmunity. Cytokine *109*, 24–28. https://doi.org/10.1016/j.cyto.2018.02.012.

38. Giunta, E.F., Barra, G., De Falco, V., Argenziano, G., Napolitano, S., Vitale, P., Zanaletti, N., Terminiello, M., Martinelli, E., Morgillo, F., et al. (2020). Baseline IFN-gamma and IL-10 expression in PBMCs could predict response to PD-1 checkpoint inhibitors in advanced melanoma patients. Sci. Rep. *10*, 17626. https://doi.org/10.1038/s41598-020-72711-2.

39. Sun, Z., Fourcade, J., Pagliano, O., Chauvin, J.M., Sander, C., Kirkwood, J.M., and Zarour, H.M. (2015). IL10 and PD-1 cooperate to limit the activity of tumor-specific CD8+ T cells. Cancer Res. *75*, 1635–1644. https://doi.org/10.1158/0008-5472.CAN-14-3016.

40. Reuben, J.M., Lee, B.N., Li, C., Gomez-Navarro, J., Bozon, V.A., Parker, C.A., Hernandez, I.M., Gutierrez, C., Lopez-Berestein, G., and Camacho, L.H. (2006). Biologic and immunomodulatory events after CTLA-4 blockade with ticilimumab in patients with advanced malignant melanoma. Cancer *106*, 2437–2444. https://doi.org/10.1002/cncr.21854.

41. Haanen, J.B.A.G., Carbonnel, F., Robert, C., Kerr, K.M., Peters, S., Larkin, J., and Jordan, K.; ESMO Guidelines Committee (2017). Management of toxicities from immunotherapy: ESMO Clinical Practice Guidelines for diagnosis, treatment and follow-up. Ann. Oncol. *28*, iv119–iv142. https://doi.org/10.1093/annonc/mdx225.

42. Mei, H.E., Leipold, M.D., and Maecker, H.T. (2016). Platinum-conjugated antibodies for application in mass cytometry. Cytometry A. *89*, 292–300. https://doi.org/10.1002/cyto.a.22778.

43. Friebel, E., Kapolou, K., Unger, S., Núñez, N.G., Utz, S., Rushing, E.J., Regli, L., Weller, M., Greter, M., Tugues, S., et al. (2020). Single-cell mapping of human brain cancer reveals tumor-specific instruction of tissue-invading leukocytes. Cell *181*, 1626–1642.e20. https://doi.org/10.1016/j.cell.2020.04.055.

44. Van Gassen, S., Gaudilliere, B., Angst, M.S., Saeys, Y., and Aghaeepour, N. (2020). CytoNorm: a normalization algorithm for cytometry data. Cytometry A. *97*, 268–278. https://doi.org/10.1002/cyto.a.23904.

45. Brummelman, J., Haftmann, C., Núñez, N.G., Alvisi, G., Mazza, E.M.C., Becher, B., and Lugli, E. (2019). Development, application and computational analysis of high-dimensional fluorescent antibody panels for single-cell flow cytometry. Nat. Protoc. *14*, 1946–1969. https://doi.org/10.1038/s41596-019-0166-2.

Please cite this article in press as: Nuñez et al., Immune signatures predict development of autoimmune toxicity in patients with cancer treated with immune checkpoint inhibitors, Med (2023), https://doi.org/10.1016/j.medj.2022.12.007

STAR★METHODS

KEY RESOURCES TABLE

REAGENT or RESOURCE	SOURCE	IDENTIFIER
Antibodies		
anti-human CD56 purified with 176Yb	BD Bioscience	Cat# 559043; RRID: AB_397180
anti-human CD21 purified with 141Pr	Biolegend	Cat# 354902; RRID: AB_11219188
anti-human CD28 purified with 143ND	Biolegend	Cat# 302902; RRID: AB_314304
anti-human CD38 purified with 147Sm	Biolegend	Cat# 303502; RRID: AB_314354
anti-human CD39 purified with 156Gd	Biolegend	Cat# 328221; RRID: AB_2563747
anti-human CD45RO purified with 159Tb	Biolegend	Cat# 304202; RRID: AB_314418
anti-human KLRG-1 purified with 163Dy	Biolegend	Cat# 368602; RRID: AB_2566256
anti-human IgD purified with 164Dy	Biolegend	Cat# 348202; RRID: AB_10550095
anti-human 2B4 purified with 166Er	Biolegend	Cat# 329502; RRID: AB_1279194
anti-human ICOS purified with 173Yb	Biolegend	Cat# 313502; RRID: AB_416326
anti-human TIGIT purified with 169Tm	Thermo Fisher	Cat# 16-9500-82; RRID: AB_10718831
anti-human CD19 142ND	Fluidigm	Cat# 3142001B; RRID: AB_2651155
anti-human CD69 144ND	Fluidigm	Cat# 3144018; RRID: AB_2687849
anti-human CD4 145ND	Fluidigm	Cat# 3145001B; RRID: AB_2661789
anti-human CD8 146ND	Fluidigm	Cat# 3146001B; RRID: AB_2687641
anti-human CD16 148ND	Fluidigm	Cat# 3148004B; RRID: AB_2661791
anti-human CD25 149Sm	Fluidigm	Cat# 3149010B; RRID: AB_2756416
anti-human HLA-DR 150ND	Fluidigm	Cat# 3150028B; RRID: N/A
anti-human CD103 151Eu	Fluidigm	Cat# 3151011B; RRID: AB_2756418
anti-human TCRgd 152Sm	Fluidigm	Cat# 3152008B; RRID: AB_2687643
anti-human CD45RA 153Eu	Fluidigm	Cat# 3153001B; RRID: AB_2802108
anti-human CD3 154Sm	Fluidigm	Cat# 3154003B; RRID: AB_2687853
anti-human CD27 155Gd	Fluidigm	Cat# 3155001B; RRID: AB_2687645
anti-human CD10 158Gd	Fluidigm	Cat# 3158011B; RRID: N/A
anti-human CD14 160Gd	Fluidigm	Cat# 3160001B; RRID: AB_2687634
anti-human CCR7 167Er	Fluidigm	Cat# 3167009A; RRID: AB_2858236
anti-human CD57 172Yb	Fluidigm	Cat# 3172009B; RRID: AB_2888930
anti-human PD-1 174Yb	Fluidigm	Cat# 3174020B; RRID: AB_2868402
anti-human CD11b 209Bi	Fluidigm	Cat# 3209003B; RRID: AB_2687654
anti-human IgG4 purified with 161Gd	Thermo Fisher	Cat# MH1542; RRID: AB_2539712
Cell-ID™ Cisplatin 195Pt	Fluidigm	Cat# 201064; RRID: N/A
anti-Biotin 161Gd	Biolegend	anti-Biotin 161Gd
anti-human FoxP3 162Dy	Fluidigm	anti-human FoxP3 162Dy
anti-human Ki-67 168Er	Fluidigm	anti-human Ki-67 168Er
anti-human EOMES purified with 165Ho	Thermo Fisher	anti-human EOMES 165Ho
anti-human CTLA-4 170Er	Fluidigm	anti-human CTLA-4 170Er
anti-human Granzyme B 171Yb	Fluidigm	anti-human Granzyme B 171Yb
anti-human Perforin 175Lu	Fluidigm	anti-human Perforin 175Lu
Cell-ID™ Intercalator-Ir 191Ir; 193Ir	Fluidigm	Cell-ID™ Intercalator-Ir 191Ir; 193Ir
anti-human CD45 BUV395	BD Bioscience	Cat# 563792; RRID: AB_2869519
anti-human HLA-DR BUV661	BD Bioscience	Cat# 612980; RRID: AB_2870252
anti-human CD45RO BUV615-p	BD Bioscience	Cat# 751167; RRID: AB_2875191
anti-human CD3 BUV805	BD Bioscience	Cat# 565515; RRID: AB_2739277
anti-human CD19 BUV737	BD Bioscience	Cat# 612756; RRID: AB_2870087
anti-human CD16 BUV496	BD Bioscience	Cat# 612944; RRID: AB_2870224
anti-human CD4 BUV563	BD Bioscience	Cat# 612912; RRID: AB_2739451
anti-human CD152 (CTLA-4) BB790-P	BD Bioscience	customized
anti-human Granzyme B AF647	BD Bioscience	Cat# 560212; RRID: AB_11154033
anti-human Ki-67 BV480	BD Bioscience	Cat# 566109; RRID: AB_2739511
Streptavidin BB630	BD Bioscience	customized

(*Continued on next page*)

Please cite this article in press as: Nuñez et al., Immune signatures predict development of autoimmune toxicity in patients with cancer treated with immune checkpoint inhibitors, Med (2023), https://doi.org/10.1016/j.medj.2022.12.007

Continued

REAGENT or RESOURCE	SOURCE	IDENTIFIER
anti-human TCR PANgd PE-Cy5	Beckman Coulter	Cat# IM2662U; RRID: N/A
anti-human CD8 BV570	Biolegend	Cat# 301038; RRID: AB_2563213
anti-human CD56 PE/Dazzle™ 594	Biolegend	Cat# 362544; RRID: AB_2565922
anti-human CD279 (PD-1) BV421	Biolegend	Cat# 329920; RRID: AB_10960742
anti-human CD27 BV650	Biolegend	Cat# 302828; RRID: AB_2562096
anti-human CD127 BV605	Biolegend	Cat# 351334; RRID: AB_2562022
anti-human IL-2 BV711	Biolegend	Cat# 500346; RRID: AB_2616639
anti-human TNFalpha BV785	Biolegend	Cat# 502948; RRID: AB_2565858
anti-human IFN-γ AF700	Biolegend	Cat# 502520; RRID: AB_528921
anti-human IL-17A APC-CY7	Biolegend	Cat# 512320; RRID: AB_10613103
anti-human EOMES FITC	Thermo Fisher	Cat# 11-4877-42; RRID: AB_2572499
anti-human FOXP3 PE	Thermo Fisher	Cat# 12-4777-42; RRID: AB_1944444
anti-human CD45RA Pe-Cy5.5	Thermo Fisher	Cat# MHCD45RA18; RRID: AB_10372221
anti-human IgG4 Biotin	Thermo Fisher	Cat# MH1542; RRID: AB_2539712
anti-human KLRG1 Pe-Cy7	Thermo Fisher	Cat# 25-9488-42; RRID: AB_2573546
anti-human CD39 PerCP-eFluor 710	Thermo Fisher	Cat# 46-0399-42; RRID: AB_10597271
anti-human TIGIT BUV395	BD Bioscience	Cat# 747845; RRID: AB_2872308
anti-human HLA-DR BUV661	BD Bioscience	Cat# 612980; RRID: AB_2870252
anti-human CCR4 BUV615-p	BD Bioscience	Cat# 613000; RRID: AB_2870269
anti-human CD3 BUV805	BD Bioscience	Cat# 565515; RRID: AB_2739277
anti-human CD39 BUV737	BD Bioscience	Cat# 612852; RRID: AB_2738919
anti-human CD27 BUV563	BD Bioscience	Cat# 741366; RRID: AB_2870866
anti-human PE CD25	BD Bioscience	Cat# 555432; RRID: AB_395826
anti-human CD152 (CTLA-4) BB790-P	BD Bioscience	customized
anti-human GZMB AF700	BD Bioscience	Cat# 560213; RRID: AB_1645453
anti-human Ki-67 BV480	BD Bioscience	Cat# 566109; RRID: AB_2739511
Streptavidin BB630	BD Bioscience	customized
anti-human CD8 BV570	Biolegend	Cat# 301038; RRID: AB_2563213
anti-human CD56 PE/Dazzle™ 594	Biolegend	Cat# 362544; RRID: AB_2565922
anti-human CD69 BV421	Biolegend	Cat# 310930; RRID: AB_2561909
anti-human CD103 Biotin	Biolegend	Cat# 350220; RRID: AB_2629646
anti-human CXCR3 BV650	Biolegend	Cat# 353729; RRID: AB_2562628
anti-human PD1 BV605	Biolegend	Cat# 329924; RRID: AB_2563212
anti-human CCR7 BV785	Biolegend	Cat# 353229; RRID: AB_2561371
anti-human CD4 Spark Blue 550	Biolegend	Cat# 344656; RRID: AB_2819979
anti-human CD45 Percp	Biolegend	Cat# 304026; RRID: AB_893337
anti-human CD45RO APC	Biolegend	Cat# 304210; RRID: AB_314426
anti-human CD38 APC-Fire 810	Biolegend	Cat# 303550; RRID: AB_2860784
anti-human CD127 BV510	Biolegend	Cat# 351332; RRID: AB_2562304
anti-human T-bet BV711	Biolegend	Cat# 644820; RRID: AB_2715766
anti-human TCF1 Alexa 488	Cell Signaling	Cat# 6444; RRID: AB_2797627
anti-human CD45RA Pe-Cy5.5	ThermoScientific	Cat# MHCD45RA18; RRID: AB_10372221
anti-human CD95 PE-Cy5	ThermoScientific	Cat# 15-0959-42; RRID: AB_11042290
anti-human KLRG1 PerCP-eFluor 710	ThermoScientific	Cat# 46-9488-42; RRID: AB_2573889
anti-human CD19 Super Bright 436	ThermoScientific	Cat# 62-0199-42; RRID: AB_2637386
anti-human CD14 Qdot800	ThermoScientific	Cat# Q10064; RRID: AB_2556449
anti-human Eomes APC-eFluor780	ThermoScientific	Cat# 47-4877-42; RRID: AB_2573982
anti-human FOXP3 Pe-Cy7	ThermoScientific	Cat# 25-4777-42; RRID: AB_2573450
Biological samples		
PBMCs from cancer patients	Kantonsspital St Gallen	N/A
Serum from cancer patients	Kantonsspital St Gallen	N/A
Serum from cancer patients	University Hospital Zurich	N/A
Serum from cancer patients	Uniklinikum Erlangen	N/A
Serum from cancer patients	Ludwig Maximilian University of Munich	N/A

(*Continued on next page*)

Please cite this article in press as: Nuñez et al., Immune signatures predict development of autoimmune toxicity in patients with cancer treated with immune checkpoint inhibitors, Med (2023), https://doi.org/10.1016/j.medj.2022.12.007

Continued

REAGENT or RESOURCE	SOURCE	IDENTIFIER
Serum from cancer patients	Krankenhaus Nordwest Frankfurt	N/A
Serum from cancer patients	University Hospital Essen	N/A
Critical commercial assays		
Olink Inflammation panel	Olink Proteomics	N/A
Chemicals, peptides, and recombinant proteins		
RPMI 1640	Seraglob	Cat# M3413; RRID: N/A
PBS	Homemade	N/A
Human TruStain FcX	BioLegend	Cat# 422302; RRID:AB_2818986
Benzonase nuclease	Sigma-Aldrich	Cat# E1014-25KU; RRID: N/A
Fetal bovine serum	GIBCO	Cat# A3160802; RRID: N/A
Penicillin Streptomycin	GIBCO	Cat# 15140-148; RRID: N/A
GlutaMAX	GIBCO	Cat# 35050-038; RRID: N/A
Phorbol 12-myristate 13-acetate	Sigma-Aldrich	Cat# P1585-1MG; RRID: N/A
Ionomycin	Sigma-Aldrich	Cat# I0634-1MG; RRID: N/A
1x Brefeldin A (Golgi Plug)	BD Bioscience	Cat# 555029; RRID:AB_2869014
1x Monensin (Golgi Stop)	BD Bioscience	Cat# 554724; RRID:AB_2869012
Zombie NIR™ Fixable Viability Kit	Biolegend	Cat# 423106; RRID: N/A
Zombie Aqua™ Fixable Viability Kit	Biolegend	Cat# 423102; RRID: N/A
Deposited data		
Mass cytometry data	This study	https://zenodo.org/record/7079638
Flow cytometry data	This study	https://zenodo.org/record/7079638
Spectral flow cytometry data	This study	https://zenodo.org/record/7079638
Olink inflammation panel data	This study	https://zenodo.org/record/7079638
Software and algorithms		
Affinity designer	Affinity	https://affinity.serif.com/de/designer/
Dplyr		https://cran.r-project.org/web/packages/dplyr/index.html
FlowJo V10.6.2.	Tree Star	https://www.flowjo.com/
FlowSOM		https://github.com/SofieVG/FlowSOM
flowStats		https://www.bioconductor.org/packages/release/bioc/html/flowStats.html
ggplot2		https://cran.r-project.org/web/packages/ggplot2/index.html
Hmisc		https://cran.r-project.org/web/packages/Hmisc/index.html
Pheatmap		https://cran.r-project.org/web/packages/pheatmap/index.html
R studio		https://www.rstudio.com/
R version 3.6.1		https://www.r-project.org/
Stats		https://CRAN.R-project.org/package=STAT
UMAP		https://github.com/lmcinnes/umap
Flowcore		https://www.bioconductor.org/packages/devel/bioc/vignettes/flowCore/inst/doc/HowTo-flowCore.pdf
Finalfit		https://cran.r-project.org/web/packages/finalfit
Forestplot		https://cran.r-project.org/web/packages/forestplot
pROC		https://cran.r-project.org/web/packages/pROC
Other		
Automated cell counter	Bio-Rad	N/A
Helious CyTOF2	Fluidigm	N/A
FACSymphony	BD Bioscience	N/A
Cytek Aurora	Cytek Biosciences	N/A

Please cite this article in press as: Nuñez et al., Immune signatures predict development of autoimmune toxicity in patients with cancer treated with immune checkpoint inhibitors, Med (2023), https://doi.org/10.1016/j.medj.2022.12.007

RESOURCE AVAILABILITY

Lead contact

Further information and requests for resources should be directed to the lead contact, Lukas Flatz (lukas.flatz@med.uni-tuebingen.de).

Materials availability

This study did not generate new, unique reagents.

Data and code availability

The codes that support these findings have been previously described.[41,42]

All data is available in a public repository (https://zenodo.org/record/7079638).

Any additional information required to reanalyze the data reported in this paper is available from the lead contact upon request.

EXPERIMENTAL MODEL AND SUBJECT DETAILS

Human samples: participant information on gender and age was self-reported. Information on gender, race and socioeconomic status was not collected. Patient information including gender and age are reported in Table S1.

METHOD DETAILS

Clinical samples

A prospective cohort study (Immunomonitoring of Immunotherapy (IMIT) study) of patients with NSCLC or melanoma who received ICI treatment was conducted across four different centers in Switzerland (Kantonsspital St Gallen, Spital Grabs, Spital Wil, and Spital Flawil) from July 1, 2016, to January, 2021. The study received approval from the Ethics Committee of Eastern Switzerland (Ethikkommission Ostschweiz, EKOS 16/079) and was conducted in accordance with the Declaration of Helsinki guidelines. Informed consent was obtained from all patients.

Patients received either nivolumab (240 mg every 2 weeks), pembrolizumab (200 mg every 3 weeks), ipilimumab (3 mg/kg every 3 weeks), atezolizumab (1200 mg every 3 weeks) or a combination of nivolumab and ipilimumab (1 mg/kg nivolumab and 3 mg/kg ipilimumab every 3 weeks, followed by nivolumab monotherapy 240 mg every 2 weeks) (Table S1). PBMCs and serum were collected at baseline (pre-therapy) and at every time point of ICI administration, and when patients experienced irAEs. For the majority of patients, blood samples taken at the onset of irAEs were collected prior to the initiation of systemic steroids. Median patient follow-up time was 618 days (mean was 703 days) and ranged from 40 days to 1689 days. All irAEs were diagnosed according to standard ESMO clinical practice guidelines.[41]

The prospective patient cohort consisted of 101 patients with NSCLC and 43 patients with melanoma. In the NSCLC group, 32 patients (32%) experienced complete or partial remission (CR/PR), 23 patients (23%) had stable disease (SD) and 44 patients (44%) had progressive disease (PD). In the melanoma group, 20 patients (48%) experienced CR/PR, 7 patients (17%) experienced SD and 15 patients (36%) had PD. The median time to tumor response evaluation was 12 weeks after the start of ICI treatment. Patients were divided into responders and non-responders, according to the following criteria: patients experiencing partial remission at the first CT scan occurring three months after therapy start, and patients with stable tumors for at least six months after therapy start were considered responders; patients with

Please cite this article in press as: Nuñez et al., Immune signatures predict development of autoimmune toxicity in patients with cancer treated with immune checkpoint inhibitors, Med (2023), https://doi.org/10.1016/j.medj.2022.12.007

progressive tumors at the first CT scan and those with stable disease that experienced progression within six months of start of therapy were considered non-responders (Table S1). For the PBMC and serum analyses samples from four different time points were used: pre-therapy (T1), one to two weeks after the start of therapy (T2), one month before the onset of the first autoimmune toxicity (T3) and the time point of the first autoimmune toxicity (T4). For patients not experiencing irAEs, T3 and T4 were selected in order to match T3 and T4 of patients experiencing irAEs as close as possible.

A prospective validation cohort was then recruited to confirm the main findings (Table S1). This validation cohort was recruited from two centers in Switzerland (St. Gallen and Zurich) and four centers in Germany (Frankfurt, Essen, Munich and Erlangen). As for the discovery cohort, the studies received ethical approval (Ethikkommission Ostschweiz, EKOS 16/079; KEK Zurich, BASEC-Nr. PB_2017-00494; Landesärztekammer Hessen, MC 288/2015; WBE/SCABIO, 11-4715; Ethikvotum München, 20-1122; Ethikvotum 195_20B Erlangen) and were conducted in accordance with the Declaration of Helsinki guidelines; informed consent was obtained from all patients. Median patient follow up time was 413 days (mean was 544 days) and ranged from 16 days to 1677 days. The median time to tumor response evaluation was 12 weeks after the start of ICI treatment. For patients receiving adjuvant therapy, response was defined as no relapse during 12 months of adjuvant therapy, while no response was defined as relapse during this time.

Ex vivo reactivation of PBMCs

Cryopreserved PBMCs from melanoma and NSCLC patients were stored in liquid nitrogen. Cells were first thawed in a 37°C water bath for 4 min and then gently resuspended in 1 mL of prewarmed complete medium [RPMI1640 (PAN biotech), 10% FCS (Biochrom), 1×penicillin/streptomycin (Life Technologies)] supplemented with 1:10,000 benzonase (Sigma-Aldrich). Cell count was calculated using an automated cell counter (Bio-Rad). PBMCs were then transferred into conical tubes containing 10 mL of complete medium, and centrifuged (7 min at 300 rcf, 24°C).

Cell stimulation and flow cytometry data acquisition

For the discovery cohort, PBMCs (10^6 cells/ml) were stimulated for 5 h with 100 ng/mL of PMA and 1 μg/mL ionomycin in the presence of 1 μL/mL GolgiPlug/GolgiStop (BD Biosciences). For both the discovery and validation cohort, cells were washed with PBS, and non-specific antibody binding was blocked using human TruStain FcX (Biolegend). Then, PBMCs were incubated for 25 min at 4C with the antibodies listed in STAR Methods section (Flow Cytometry or Spectral Flow Cytometry). Prior to intracellular labeling, cells were fixed and permeabilized with fixation/permeabilization solution (Thermo Fisher), according to the manufacturer's instructions. Cells were then incubated overnight at 4C with the antibodies listed in STAR Methods section. For the discovery and validation cohort, data were acquired with a BD Bioscience FACSymphony or Cytek Aurora flow cytometer, respectively, and analyzed using FlowJo Software (version 10, TreeStar Inc.).

Cellular barcoding and mass cytometry acquisition

A unique three-out-of-nine metal barcode scheme was used to perform the living cell barcode.[42,43] The metals 104Pd, 105Pd, 106Pd, 108Pd, 110Pd, 113In, 115In and 181Ta (Trace Sciences International) were conjugated to purified human anti-CD45 antibody (Biolegend) in-house using the Maxpar X8 Chelating Polymer Kit (Fluidigm), according to the manufacturer's instructions. In addition, a yttrium (CD45 89Y) (Fluidigm) pre-conjugated anti-human antibody was used. The cells

Please cite this article in press as: Nuñez et al., Immune signatures predict development of autoimmune toxicity in patients with cancer treated with immune checkpoint inhibitors, Med (2023), https://doi.org/10.1016/j.medj.2022.12.007

were then incubated on ice in RPMI-1640 supplemented with 5% FCS and a unique combination of metal-labeled anti-CD45 antibodies. The samples were then washed twice in PBS and pooled for antibody surface labeling. Then, PBMCs were incubated for 25 min with the antibodies listed STAR Methods section. Prior to intracellular labeling, cells were fixed and permeabilized with fixation/permeabilization solution (Thermo Fisher), according to the manufacturer's instructions. Cells were then incubated for 25 min with the antibodies listed in STAR Methods section. The cells were then incubated in 4% PFA (Electron Microscopy Sciences) overnight. Before acquisition, cells were resuspended in 1:3000 Cell-IDTM Intercalator-Ir (Fluidigm) + Maxpar Fix and Perm Buffer (Fluidigm). The cells were then washed with 1x PBS and ddH2O and diluted to 1.5–106 cells/ml in ddH2O containing 10% EQ Four Element Calibration Beads (Fluidigm). Data were acquired with a Helious CyTOF2 (Fluidigm) and analyzed using FlowJo Software (version 10, TreeStar Inc.).

High-dimensional flow cytometry and mass cytometry analysis

High dimensional mass cytometry (CyTOF) data were acquired in two batches. For high-dimensional flow cytometry analysis, raw datasets were compensated, doublets were excluded using Gaussian discrimination based on FSC-A and FSC-H, followed by dead cell exclusion using Zombie Aqua expression assessed by with. For high-dimensional CyTOF, raw datasets were normalized using the MATLAB version of the Normalizer tool. Cells were gated on positive Event length and DNA using 191Ir and 193Ir channels by manual gating, followed by cell dead discrimination based on 195Pt expression. Doublets were excluded using Gaussian discrimination channels including Center, Offset, Width and Residual. Next, data were concatenated and de-barcoded using boolean gating.

Live cell data from high-dimensional flow cytometry and CyTOF data from every individual patient were manually exported from FlowJo and uploaded into Rstudio (R software environment, version R4) using "flowCore" packages. Both datasets were normalized using Cytonorm,[44] employing arcsinh transformation and quantile normalization.[45]

To obtain an unbiased overview, we systematically reduced the flow cytometry data to two dimensions by applying uniform manifold approximation (UMAP, R package "umap"). All cells were clustered using the FlowSOM algorithm (R package "FlowSOM") in conjunction with consensus clustering (R package "ConsensusClusterPlus") and subsequently manually annotated.[42]

Proteomics

The proteomics analysis of patient serum samples was carried out using the Olink platform "Target 96 Inflammation panel" (https://www.olink.com/products/inflammation/). This panel provides a high-throughput, multiplex immunoassay enabling analysis of 92 inflammation-related protein biomarkers across 88 samples simultaneously, using the Proximity Extension Assay (PEA) technology. In brief, each protein is bound by a matched pair of antibodies, coupled to unique and partially complementary oligonucleotides. When the DNA coupled to the two antibodies is brought into close proximity, it hybridizes. Only the correctly hybridized tags are extended to an amplicon by quantitative real-time PCR, with a unique sequence for each protein. This requirement for dual antibody binding paired with DNA barcoding provides exceptional readout specificity. The software then reports the relative concentrations of proteins. More specifically, the proteomics data is released in a normalized protein expression (NPX) format, which is Olink's arbitrary unit, in Log2 scale. NPX data allows users to identify changes for individual protein

Please cite this article in press as: Nuñez et al., Immune signatures predict development of autoimmune toxicity in patients with cancer treated with immune checkpoint inhibitors, Med (2023), https://doi.org/10.1016/j.medj.2022.12.007

levels across the sample and to identify protein signatures. The higher the NPX value, the higher the protein concentration. As NPX is in a log2 scale, a 1 NPX difference means a doubling of protein concentration. The fold change from T1 to T2 of serum proteins was calculated by exponentiating NPX with base 2 (2^x) and then diving the value at T2 by T1.

QUANTIFICATION AND STATISTICAL ANALYSIS

All statistical analyses were performed using R version 4.0.1 (R Core Team 2020). All violin plots are presented as the quantile 0.25, 0.5 and 0.75. N represents the number of patients per group. Frequencies of immune populations and cytokines values were compared with the non-parametric Mann–Whitney–Wilcoxon test on unpaired data (Figures 1D, 1E, 2H, 3A, 3B, 4D, and 4E). For longitudinal data (same patient before and after the treatment) the Mann-Whitney-Wilcoxon test paired was used (Figures 1F, 2C, 2D, and 4C). Correction for multiple hypothesis testing with the Benjamini-Hochberg method was used. These tests were two-tailed and performed with ggpubr R package. To calculate the differences between the six subgroups of patients, the Kruskal-Wallis test (KWT) was used (Figures 1D and 1E). For correlation measurements, we used a Pearson regression model by applicating the *lm*() and *summary*() functions (Figure 2G). For logistic regression, receiver operating characteristic (ROC) and Cox proportional-hazards model of the time to irAE were calculated using the differences between patients with toxicity and without toxicity obtained by cytometry and proteomics (baseline and one to two weeks after the initiation of treatment, Figures 3C and 3D). Logistic regression, ROC curve, univariate and multivariate calculations were performed in R using the "finalfit", "forestplot", "ISLR" and "pROC" packages, respectively. p values of less than 0.05 were considered significant and are indicated by the numerical value on the respective graphs. Detailed information on statistical analysis can be found in the accompanying figure legends.